

Collision between chemically driven self-propelled drops

Shunsuke Yabunaka¹ and Natsuhiko Yoshinaga^{2,3,†}

¹Yukawa Institute for Theoretical Physics, Kyoto University, Kitashirakawa Oiwake-Cho, Kyoto, 606-8502, Japan

²WPI – Advanced Institute for Materials Research, Tohoku University, Sendai 980-8577, Japan

³MathAM-OIL, AIST, Sendai 980-8577, Japan

(Received 2 April 2016; revised 28 July 2016; accepted 12 September 2016;
first published online 30 September 2016)

We use analytical and numerical approaches to investigate head-on collisions between two self-propelled drops described as a phase separated binary mixture. Each drop is driven by chemical reactions that isotropically produce or consume the concentration of a third chemical component, which affects the surface tension of the drop. The isotropic distribution of the concentration field is destabilized by motion of the drop, which is created by the Marangoni flow from the concentration-dependent surface tension. This symmetry-breaking self-propulsion is distinct from other self-propulsion mechanisms due to its intrinsic polarity of squirmers and self-phoretic motion; there is a bifurcation point below which the drop is stationary and above which it moves spontaneously. When two drops are moving in the opposite direction along the same axis, their interactions arise from hydrodynamics and concentration overlap. We found that two drops exhibit either an elastic collision or fusion, depending on the distance from their bifurcation point, which may be controlled, for example, by viscosity. An elastic collision occurs when there is a balance between dissipation and the injection of energy by chemical reactions. We derive the reduced equations for the collision between two drops and analyse the contributions from the two interactions. The concentration-mediated interaction is found to dominate the hydrodynamic interaction for a head-on collision.

Key words: interfacial flows (free surface), low-Reynolds-number flows, propulsion

1. Introduction

In biological systems, cells and microorganisms are moving spontaneously and autonomously by consuming energy from adenosine triphosphate (ATP) hydrolysis. The size and swimming speed of bacteria are small, and their self-propulsion is described by low Reynolds number hydrodynamics. In an attempt to capture the generic mechanism of the self-propulsion, various mathematical models have been investigated. One of these is the squirmer model, which considers the flow field created by the beating of cilia on the body of a microorganism and/or the deformation

† Email address for correspondence: yoshinaga@wpi-aimr.tohoku.ac.jp

of its body surface (Lighthill 1952; Blake 1971). The problem then becomes a matter of solving the Stokes equation under the boundary conditions of finite velocity on the surface of the body in the normal and/or tangential directions. The translational and angular velocities of a single squirmer are well understood (Stone & Samuel 1996). Apart from that model, there have been several attempts to find other classes of self-propulsion. The simplest extension of the model is to include an additional scalar field such as the concentration, electric or temperature field. A Janus particle, which is an asymmetric particle with two different surface properties, creates a gradient of the field around the particle, and thus, in turn, causes it to move spontaneously (Paxton *et al.* 2004; Howse *et al.* 2007; Jiang, Yoshinaga & Sano 2010). This motion is similar to phoresis, except that the gradient is self-generated instead of imposed. This mechanism is thus called self-phoresis.

The squirmer and Janus particles have intrinsic asymmetry, and therefore the swimming direction is set by the polar direction of the asymmetry of each particle. This simplifies the problem: there is a linear relation between the self-propulsion speed and the magnitude of the asymmetry. This idea may also be extended toward self-propulsion of a geometrically asymmetric object with a uniform surface property (Tsemakh, Lavrenteva & Nir 2004; Shklyaev, Brady & Crdova-Figueroa 2014). On the other hand, cells often break symmetry to choose the direction of motion (Yam *et al.* 2007). This phenomenon is not captured by the squirmer and Janus particles, and therefore another class of self-propulsion must be considered. As a step in this direction, various mathematical models that include the internal polarity field have been proposed (Shao, Rappel & Levine 2010; Tjhung, Marenduzzo & Cates 2012; Ziebert, Swaminathan & Aranson 2012). In these models, it has been observed that spontaneous symmetry-breaking results in directional motion.

Along this line, it was recently found that non-living chemically driven systems exhibit self-propulsion (Toyota *et al.* 2009; Thutupalli, Seemann & Herminghaus 2011; Izri *et al.* 2014). In these systems, a drop may produce or consume chemical molecules in such a way that the system is away from an equilibrium state. The flux couples with the motion and results in an asymmetric concentration distribution. Once the symmetry is broken, the surface tension becomes anisotropic and this creates flow both inside and outside the drop. This motion, which occurs along the given gradient of concentration and/or temperature fields, is known as the Marangoni effect (Fedosov 1956; Young, Goldstein & Block 1959). The self-propulsive motion using the Marangoni effect resulting from a chemical reaction was first proposed as a reactive drop (Ryazantsev 1985), and later its mechanism was theoretically reformulated as a bifurcation phenomena (Yabunaka, Ohta & Yoshinaga 2012; Yoshinaga *et al.* 2012; Yoshinaga 2014). In these studies, the reduced nonlinear equations were derived from the coupled advection–diffusion and hydrodynamic equations. A similar idea was considered for the auto-phoretic motion, which is the self-phoretic motion of a Janus particle due to a nonlinear coupling of an isotropic chemical reaction and advection (Michelin, Lauga & Bartolo 2013).

Although the self-propulsion of an isolated particle/drop is well understood, there is still only a limited understanding of the interactions between them. There have been intensive numerical studies of interactions between squirmers (Ishikawa, Simmonds & Pedley 2006) and between a squirmer and a wall (Spagnolie & Lauga 2012). In particular, understanding of the squirmer/wall system has recently increased, and numerical simulations have revealed the bound state near the wall (Li & Ardekani 2014). These results are consistent with those from an analysis of the equation of

motion of a squirmer, using a technique for analysing dynamical systems (Ishimoto & Gaffney 2013). Even for Janus particles, numerical simulations near a wall have only been performed very recently (Uspal *et al.* 2015).

In this work, we discuss the interaction between self-propelled drops. In particular, we focus on head-on collisions between two drops. As we will discuss, the interaction arises from hydrodynamics and a concentration overlap. The hydrodynamic interaction has been discussed in terms of the squirmer model, in which only the velocity field is treated. The concentration overlap has been discussed in the context of reaction–diffusion systems; in that case, the concentration fields are analysed without considering the hydrodynamics, and thus mechanics does not play a role (Ohta, Kiyose & Mimura 1997; Ohta 2001; Bode *et al.* 2002; Nishiura, Teramoto & Ueda 2003; Ei, Mimura & Nagayama 2006). The primary questions are which effect dominates the interaction and when do cross-overs occur. To answer these questions, we consider the theory for two interacting drops that are separated far away from each other. This is an extension of the theory for a single drop discussed in Yabunaka *et al.* (2012), Yoshinaga (2014). Other studies (Golovin, Nir & Pismen 1995; Lavrenteva, Leshansky & Nir 1999) have used a boundary-value approach to investigate the interaction that arises from hydrodynamics and the concentration (or heat) field. Our model shares a similar philosophy, although we focus on the equations of motion of a reduced description and drops with unsteady motion, rather than stationary speed. The main difference is that we use a diffuse-interface approach, and because of this, both analytical and numerical solutions become tractable. We will discuss the similarities and differences in § 8.

We also develop numerical simulations of isolated as well as interacting drops. This enables us to investigate the effect of advection of the chemical component; a complete analytical investigation of this has not been previously performed (Yabunaka *et al.* 2012; Yoshinaga 2014). We confirm that the convection of the chemical component does not change the essential bifurcation of a single drop, but it suppresses the drift instability; this supports previously presented theories (Yabunaka *et al.* 2012; Yoshinaga 2014). For interacting drops, we will numerically investigate the dynamics of collisions; this complements our theoretical calculations.

The interaction between two self-propelled particles is distinct from that seen in conventional passive systems, where particles and drops are driven by external forces (Jeffrey & Onishi 1984). The dominant hydrodynamic interaction in the far field does not arise from a Stokeslet but from a source doublet or a stresslet depending on the mode ($l = 1$ or $l = 2$) for the expansion of the slip velocity, as expressed by spherical harmonics (Lauga & Powers 2009; Pak & Lauga 2014). In addition, our system is different from either the squirmer or the Janus particle; it does not have a specific intrinsic polarity, but polarity spontaneously appears when the bifurcation parameter exceeds a threshold value. Consequently, the direction of motion of a drop may change without rotation.

In the remaining sections, we formulate a model for chemically driven self-propulsion that uses the Marangoni effect. To prepare for the main parts, in § 2, we compute the flow field and resulting velocity of a drop under a given distribution of the surface tension. In § 3, we summarize the spontaneous motion of an isolated drop. In § 4, we derive the hydrodynamic and concentration-mediated interactions between two drops, and the equations of motion for two interacting drops are formulated in § 5. Numerical results for isolated and colliding drops are presented in §§ 6 and 7, respectively. We compare the numerical results with our theoretical analysis of § 4. We conclude with § 8, which summarizes our results.

2. An isolated drop under a given concentration gradient

Before discussing the interaction between spherical drops, we first calculate the flow field around a spherical drop driven by an arbitrary distribution of the surface tension. The axisymmetric flow field around the drop has been studied (Young *et al.* 1959; Levan 1981; Kitahata *et al.* 2011). Here we do not assume that the system is axisymmetric; thus, instead of expanding the surface tension in terms of Legendre polynomials, we use spherical harmonics:

$$\gamma(\theta, \varphi) = \sum_{l,m} \gamma_{lm} Y_l^m(\theta, \varphi). \tag{2.1}$$

The velocity fields inside and outside the drop are expanded as follows:

$$\mathbf{v}^{(i)} = \sum_{l,m} \mathbf{v}_{lm}^{(i)} = \sum_{l,m} [f_{lm}^{(i)}(r) \mathbf{Y}_{lm}(\theta, \varphi) + g_{lm}^{(i)}(r) \boldsymbol{\Psi}_{lm}(\theta, \varphi)] \tag{2.2}$$

$$\mathbf{v}^{(o)} = \sum_{l,m} \mathbf{v}_{lm}^{(o)} = \sum_{l,m} [f_{lm}^{(o)}(r) \mathbf{Y}_{lm}(\theta, \varphi) + g_{lm}^{(o)}(r) \boldsymbol{\Psi}_{lm}(\theta, \varphi)], \tag{2.3}$$

where the outer and inner fields are indicated by the superscripts (*o*) and (*i*), respectively, and the vector spherical harmonics are defined by using the scalar spherical harmonics $Y_l^m(\theta, \varphi)$, as follows:

$$\mathbf{Y}_{lm} = Y_l^m \hat{\mathbf{r}} \tag{2.4}$$

$$\boldsymbol{\Psi}_{lm} = r \nabla Y_l^m, \tag{2.5}$$

where $\hat{\mathbf{r}}$ is a unit normal vector. Since the flow field is driven by the gradient of the surface tension, one of the vector spherical harmonics, $\boldsymbol{\Phi}_{lm} = \mathbf{r} \times \nabla Y_l^m$, which is in the tangential direction perpendicular to $\boldsymbol{\Psi}_{lm}$, does not appear in this expansion. Note that $f_{lm}(r)$ and $g_{lm}(r)$ are determined from the boundary conditions, as discussed below.

We consider a spherical drop that is moving with velocity \mathbf{u} in an arbitrary direction. At any point (θ, φ) on the drop surface, the velocity is expressed as

$$\mathbf{u} = \sum_m u_m (\mathbf{Y}_{1,m}(\theta, \varphi) + \boldsymbol{\Psi}_{1,m}(\theta, \varphi)), \tag{2.6}$$

which can be expressed in the Cartesian coordinates as (see (2.11))

$$\mathbf{u} = \left(\sqrt{\frac{3}{4\pi}} \frac{u_{-1} - u_1}{\sqrt{2}}, i \sqrt{\frac{3}{4\pi}} \frac{-u_{-1} - u_1}{\sqrt{2}}, \sqrt{\frac{3}{4\pi}} u_0 \right). \tag{2.7}$$

We will assume the velocity of the drop is sufficiently slow that the Reynolds number is near zero, and thus it satisfies the Stokes equation except over the surface of the drop $r = R$

$$\eta^{(i)} \nabla^2 \mathbf{v}^{(i)} - \nabla p^{(i)} = 0, \tag{2.8}$$

$$\eta^{(o)} \nabla^2 \mathbf{v}^{(o)} - \nabla p^{(o)} = 0. \tag{2.9}$$

The pressure p is determined from the incompressibility condition

$$\nabla \cdot \mathbf{v} = 0. \tag{2.10}$$

The boundary conditions on $r = R$ are

$$\mathbf{v}^{(o)} \cdot \hat{\mathbf{r}} = \mathbf{v}^{(i)} \cdot \hat{\mathbf{r}} = \mathbf{u} \cdot \hat{\mathbf{r}} \quad (2.11)$$

$$\mathbf{v}^{(o)} \cdot \hat{\mathbf{t}} = \mathbf{v}^{(i)} \cdot \hat{\mathbf{t}} \quad (2.12)$$

$$\sigma_{nt}^{(i)}(R)\hat{\mathbf{t}} = \sigma_{nt}^{(o)}(R)\hat{\mathbf{t}} + \frac{1}{R}\nabla_s\gamma, \quad (2.13)$$

where $\hat{\mathbf{t}}$ is the unit tangent vectors. The conditions (2.11) and (2.12) are continuity of the velocity field across the interface, and (2.13) implies that the forces are balanced at the interface, that is, the jump of shear stress across the interface due to the force created by the inhomogeneous surface tension (Scriven 1960). The system is force free; there is no mechanical force acting on the drop,

$$\mathbf{F} = \int dS \sigma^{(o)}(R) \cdot \mathbf{n} = 0, \quad (2.14)$$

where the integral is taken over the surface of the drop. The stress balance in the normal direction is automatically satisfied for the $l=1$ mode and determines the shape of the drop for $l \geq 2$.

The solution of the Stokes equations for this system, (2.8) and (2.9), can be decomposed into two parts: one for $l=1$ and the other for $l \geq 2$. For $l=1$,

$$\mathbf{v}_{1,m}^{(i)} = u_m \left(\left[-\frac{3}{2} \left(\frac{r}{R} \right)^2 + \frac{5}{2} \right] \mathbf{Y}_{1,m} + \left[-3 \left(\frac{r}{R} \right)^2 + \frac{5}{2} \right] \boldsymbol{\Psi}_{1,m} \right) \quad (2.15)$$

$$\mathbf{v}_{1,m}^{(o)} = u_m \left[\left(\frac{R}{r} \right)^3 \mathbf{Y}_{1,m} - \frac{1}{2} \left(\frac{R}{r} \right)^3 \boldsymbol{\Psi}_{1,m} \right] \quad (2.16)$$

$$p^{(o)} = 0 \quad (2.17)$$

$$p^{(i)} = - \sum_m \frac{10\eta^{(i)}\gamma_{1,m}}{R(3\eta^{(i)} + 2\eta^{(o)})} \frac{r}{R} Y_1^m(\theta, \varphi) = - \sum_m \frac{15\eta^{(i)}u_m}{R} \frac{r}{R} Y_1^m(\theta, \varphi) \quad (2.18)$$

and for $l \geq 2$

$$\begin{aligned} \mathbf{v}_{l,m}^{(i)} = & \frac{\gamma_{lm}}{2(\eta^{(i)} + \eta^{(o)})(2l+1)} \left(l(l+1) \left[\left(\frac{r}{R} \right)^{l+1} - \left(\frac{r}{R} \right)^{l-1} \right] \mathbf{Y}_{lm} \right. \\ & \left. + \left[-(l+1) \left(\frac{r}{R} \right)^{l-1} + (l+3) \left(\frac{r}{R} \right)^{l+1} \right] \boldsymbol{\Psi}_{lm} \right) \end{aligned} \quad (2.19)$$

$$\begin{aligned} \mathbf{v}_{l,m}^{(o)} = & \frac{\gamma_{lm}}{2(\eta^{(i)} + \eta^{(o)})(2l+1)} \left(l(l+1) \left[\left(\frac{R}{r} \right)^l - \left(\frac{R}{r} \right)^{l+2} \right] \mathbf{Y}_{lm} \right. \\ & \left. + \left[-(l-2) \left(\frac{R}{r} \right)^l + l \left(\frac{R}{r} \right)^{l+2} \right] \boldsymbol{\Psi}_{lm} \right) \end{aligned} \quad (2.20)$$

$$p^{(o)} = \sum_{l,m} \frac{\eta^{(o)}\gamma_{lm}}{R(\eta^{(i)} + \eta^{(o)})} \frac{l(2l-1)}{2l+1} \left(\frac{R}{r} \right)^{l+1} Y_l^m(\theta, \varphi) \quad (2.21)$$

$$p^{(i)} = \sum_{l,m} \frac{\eta^{(i)}\gamma_{lm}}{R(\eta^{(i)} + \eta^{(o)})} \frac{(l+1)(2l+3)}{2l+1} \left(\frac{r}{R} \right)^l Y_l^m(\theta, \varphi). \quad (2.22)$$

Because of the force-free condition, the velocity field for $l = 1$ decays as $1/r^3$ and not as $1/r$. This occurs because the motion is not driven by the Stokeslet but by the quadrupole (source dipole). The velocity of the drop is

$$u_m = -\frac{2\gamma_{1,m}}{3(3\eta^{(i)} + 2\eta^{(o)})}. \quad (2.23)$$

The axisymmetric case corresponds to $\gamma_{l,m} = 0$ for $m \neq 0$. This result is consistent with that of Young *et al.* 1959 (except for typographical errors; see Levan 1981, Kitahata *et al.* 2011). Note that the coefficient may depend on the definition of the normalization factor in the spherical harmonics.

3. Self-propelled motion of a single drop

In this section, we summarize the self-propelled motion of an isolated drop. The details for the analysis of this model can be found in Yabunaka *et al.* (2012). We consider the dynamics of the concentration field, $c(\mathbf{r})$, of a third dilute component

$$\frac{\partial c}{\partial t} + \mathbf{v} \cdot \nabla c = D\nabla^2 c - \kappa(c - c_\infty) + A\Theta(R - |\mathbf{r} - \mathbf{r}_G|). \quad (3.1)$$

The system is driven away from equilibrium, where the drop is stationary, by the source term described by the step function $\Theta(x)$ with the coefficient A . When $A > 0$, the drop produces chemical molecules, while when $A < 0$, the drop consumes them. Note that we do not use the comoving frame with the drop; therefore, the advection term in (3.1) describes only the advection due to the flow. In a comoving frame, there will be an additional contribution due to the fact that the drop is moving. In our model, this effect is included in the last term in (3.1).

Based on the diffuse-interface model (Hohenberg & Halperin 1977; Anderson, McFadden & Wheeler 1998), we describe the drop as a binary mixture, where $\phi = 1$ inside the drop and $\phi = -1$ outside. The dynamics is given by the Cahn–Hilliard equation with advection:

$$\frac{\partial \phi}{\partial t} + \mathbf{v} \cdot \nabla \phi = \nabla \cdot L\nabla \frac{\delta F}{\delta \phi}, \quad (3.2)$$

where the mobility L is assumed to be constant. The free energy has a double-well type potential:

$$F = \int_{\Omega} \left[-\frac{1}{2}\phi^2 + \frac{1}{4}\phi^4 + \frac{B(c)}{2}|\nabla\phi|^2 \right], \quad (3.3)$$

where Ω is the entire domain of the system. The interfacial energy is dependent on the concentration field $c(\mathbf{r})$. We assume the linear relation

$$B(c) = B_0 + B_1c(\mathbf{r}), \quad (3.4)$$

which is characterized by two parameters, B_0 and B_1 . The benefit of this approach is that we do not need to solve the Stokes equation with moving boundary conditions. The force acting on the fluid is given by

$$\mathbf{f} = -\phi\nabla \frac{\delta F}{\delta \phi} - c\nabla \frac{\delta F}{\delta c}; \quad (3.5)$$

this is generated by the surface tension and thus localises at the interface between the drop and the surrounding fluid. The force can be expressed in divergence form as

$$\mathbf{f} = \nabla \cdot \Pi, \quad (3.6)$$

where the stress is

$$\Pi_{ij} = B(c) \nabla_i \phi \nabla_j \phi + \text{isotropic terms}. \quad (3.7)$$

The isotropic terms merely modify the reference pressure and thus we will not discuss them further. In the thin-interface limit, the concentration in the region of the diffused interface (in bulk) can be represented by the surface concentration. Then, (3.4), expressing the gradient energy at a given bulk concentration, generally leads to a nonlinear dependence of the surface tension on the surface concentration. However, the surface tension can be linearly expanded with respect to the deviation from a constant value c_0 of the surface concentration, provided that the deviation across the entire surface is small:

$$\gamma(c_l) = \gamma(c_0) + \left. \frac{\partial \gamma(c_0)}{\partial c_l} (c_l - c_0) \right|_{r=R}, \quad (3.8)$$

where c_l represents the surface concentration. We may also be able to consider a more realistic dependence by replacing the functional form in (3.4) with a logarithmic function.

Instead of (2.8) and (2.9), we solve the following single Stokes equation with the force \mathbf{f} for the entire space under the incompressibility condition $\nabla \cdot \mathbf{v} = 0$:

$$\eta \nabla^2 \mathbf{v} - \nabla p + \mathbf{f} = 0. \quad (3.9)$$

We also assume $\eta^{(o)} = \eta^{(i)}$.

As discussed in Yabunaka *et al.* (2012), this model leads to the following reduced description:

$$m \frac{d\mathbf{u}}{dt} = (-\tau_c + \tau) \mathbf{u} - g\mathbf{u}|\mathbf{u}|^2. \quad (3.10)$$

In deriving this equation, they assumed the following: (i) the migration of the drop due to the diffusion is much slower than that due to the flow field, (ii) the contribution due to the deformation of the drop is negligible and (iii) the convective term in (3.1) does not qualitatively affect the bifurcation. Assumption (i) can be justified when $R \gg (L\eta_0)^{1/2}$ by estimating the migration velocity due to the gradient of the concentration c (Yabunaka *et al.* 2012; Bhagavatula, Jasnow & Ohta 1997). Assumption (ii) is justified when $\gamma_c A / (\gamma \kappa) \ll 1$ (Yoshinaga 2014).

Here the velocity and time are rescaled as follows:

$$\frac{\mathbf{u}}{D\beta} \rightarrow \mathbf{u} \quad (3.11)$$

$$\kappa t \rightarrow t. \quad (3.12)$$

The length is also rescaled by the inverse length β , which is defined as follows:

$$\beta = \sqrt{\frac{\kappa}{D}}. \quad (3.13)$$

The coefficients m , τ and g are dependent only on βR . Note that (3.10) is characterized by the single parameter

$$\tau_c = \frac{15\eta D^2 \beta^3}{2\gamma_c A}. \tag{3.14}$$

The drop is stationary for $\tau < \tau_c$, which occurs when the rate of the chemical reaction is small ($A \ll 1$) or the viscosity is high ($\eta \gg 1$). At $\tau = \tau_c$, bifurcation occurs, and the drop starts to move. Solving (3.10), the speed of the drop is

$$u = |\mathbf{u}| = \begin{cases} 0 & \text{for } \tau < \tau_c \\ \frac{u_0 e^{t/s_r}}{\sqrt{1+(e^{2t/s_r}-1)\frac{u_0^2}{u_{st}^2}}} & \text{for } \tau \geq \tau_c, \end{cases} \tag{3.15}$$

where the relaxation time s_r and the steady velocity u_{st} are

$$s_r = \frac{m}{\tau - \tau_c} \tag{3.16}$$

$$u_{st} = \sqrt{\frac{m}{gs_r}}. \tag{3.17}$$

Note that, as the non-dimensional reaction rate τ_c approaches τ , the relaxation time s_r diverges. It can be shown that, near the bifurcation point, the surface concentration deviation is very small across the entire region of the diffused interface; this justifies the assumption made for (3.8).

4. Interacting drops

When N drops are placed at disconnected positions, the concentration field is described by

$$\frac{\partial c}{\partial t} + \mathbf{v} \cdot \nabla c = D\nabla^2 c - \kappa(c - c_\infty) + \sum_{i=1}^N A_i \Theta(R_i - |\mathbf{r} - \mathbf{r}_{G,i}|), \tag{4.1}$$

where A_i , R_i and $\mathbf{r}_{G,i}$ are the source strength, size and centre of mass of the i th drop, and c_∞ is the concentration at infinity. Here we consider $N = 2$ drops of the same mean size of drops, $R_1 = R_2 = R_0$, and we set $c_\infty = 0$. We assume a sufficiently large bare surface tension γ_0 , so that the shape of the drop is always spherical. We neglect the advection term $\mathbf{v} \cdot \nabla c$ in (4.1) until § 6, where its effect will be discussed.

The velocity of each drop is given by Kawasaki & Ohta (1983), Yabunaka *et al.* (2012)

$$\mathbf{u} = \frac{1}{V} \int v_n \mathbf{R} dS, \tag{4.2}$$

where $V = 4/3\pi R_0^3$. Note that the velocity is different from that for an isolated self-propelled drop; this is due to the concentration field \mathbf{u}_c (see figure 2) and the hydrodynamic interaction \mathbf{u}_h . The velocity can be expressed as

$$\mathbf{u} = \mathbf{u}_0 + \mathbf{u}_c + \mathbf{u}_h, \tag{4.3}$$

where \mathbf{u}_0 is the contribution from an isolated drop. In the following sections, we will compute \mathbf{u}_h (§ 4.1) and $\mathbf{u}_0 + \mathbf{u}_c$ (§ 4.2).

4.1. Hydrodynamic interaction

First, we consider the hydrodynamic interaction. By assuming that the two drops are far away from each other, we may replace the contribution of the hydrodynamic interaction \mathbf{u}_h in (4.3) by the flow field created by the second drop: using Faxen's law (Hetsroni & Haber 1970), the hydrodynamic interaction can be expressed in terms of the flow field $\mathbf{v}^{(2)}$ generated by the second drop, as follows:

$$\mathbf{u}_h = \mathbf{v}^{(2)}|_{r=r_1} + O(\nabla^2 \mathbf{v}^{(2)}|_{r=r_1}). \quad (4.4)$$

The velocity is evaluated at the centre of the first drop. Because of the Laplacian operating on the velocity field, the second term is negligible compared with the first term when the distance between the two drops is large, that is, $r_{12} \gg R$. Near the drift bifurcation point (distance ϵ), the velocity of the second drop is as $u^{(2)} \sim \epsilon$, and the surface tension scales as $\gamma_{l,m} \sim \epsilon^l$. The velocity field decays as $1/r^3$ for $l=1$ and as $1/r^2$ for $l=2$. Therefore, it suffices to consider $l=1$ and $l=2$. The flow created by the second drop is

$$\mathbf{v}_{1,m}^{(1)} \simeq u_m^{(2)} \left[\left(\frac{R_0}{r_{12}} \right)^3 \mathbf{Y}_{1,m}(\pi - \theta_{12}, \pi + \varphi_{12}) - \frac{1}{2} \left(\frac{R_0}{r_{12}} \right)^3 \boldsymbol{\Psi}_{1,m}(\pi - \theta_{12}, \pi + \varphi_{12}) \right] \quad (4.5)$$

$$\mathbf{v}_{2,m}^{(1)} \simeq \frac{3\gamma_{2,m}^{(2)}}{5(\eta^{(i)} + \eta^{(o)})} \left(\frac{R_0}{r_{12}} \right)^2 \mathbf{Y}_{2,m}(\pi - \theta_{12}, \pi + \varphi_{12}), \quad (4.6)$$

where θ_{12} and φ_{12} are the polar and azimuthal angles of $\mathbf{r}_2 - \mathbf{r}_1$, respectively. Here, $\mathbf{v}_{1,m}^{(1)}$ is the quadrupole flow created by the second drop perturbing the first drop. This flow decays as $1/r_{12}^3$. The dipolar flow generated by the second drop is $\mathbf{v}_{2,m}^{(1)}$, which decays as $1/r_{12}^2$. It should be noted that unlike squirmer and Janus particles, the far-field flow is not necessarily dominated by the dipolar flow. This is because the second mode of the surface tension $\gamma_{2,m}^{(2)}$ associated with the ellipsoidal concentration field becomes small near the critical point of the drift bifurcation (Yoshinaga 2014).

4.2. Concentration-mediated interaction

Next, we consider the interaction between two drops due to overlap of the concentration field. We follow the approach in Ohta *et al.* (1997), Ohta (2001) (see figure 2). In Fourier space, (4.1) is

$$\frac{\partial c_q}{\partial t} = -D(q^2 + \beta^2)c_q + H_q, \quad (4.7)$$

where the source term H_q is

$$H_q = A_1 S_q^{(1)} e^{iq \cdot r_{G,1}} + A_2 S_q^{(2)} e^{iq \cdot r_{G,2}} \quad (4.8)$$

and

$$S_q^{(1)} = S_q^{(2)} = S_q = 4\pi \frac{\sin(qR_0) - qR_0 \cos(qR_0)}{q^3} = \frac{4\pi R_0^2}{q} j_1(qR_0). \quad (4.9)$$

The first term in (4.8) corresponds to the production of chemicals from the first drop (when $A_1 > 0$) while the second term corresponds to production from the second drop (when $A_2 > 0$). Here $j_n(x)$ for $n=0, 1, 2, \dots$ are spherical Bessel functions, as defined

in (A 2). As in Yabunaka *et al.* (2012), the solution of (4.7) is expanded close to the critical point of the drift bifurcation, that is, for $\epsilon = u/(D\beta) \ll 1$,

$$c_q = \frac{G_q}{D} H_q - \frac{G_q^2}{D^2} \frac{\partial H_q}{\partial t} + \frac{G_q^3}{D^3} \frac{\partial^2 H_q}{\partial t^2} - \frac{G_q^4}{D^4} \frac{\partial^3 H_q}{\partial t^3} + \dots, \tag{4.10}$$

where we use the Green’s function

$$G_q = \frac{1}{q^2 + \beta^2}. \tag{4.11}$$

Note that the time derivative of H_q generate the velocity of the first or second drop (and their time derivative). After performing inverse Fourier transformation of (4.10), the concentration c_I at the interface of the first drop can be expanded as

$$c_I = c_I^{(0)}(\mathbf{r}_{G,1} + \mathbf{s}) + c_I^{(1)}(\mathbf{r}_{G,1} + \mathbf{s}) + c_I^{(2)}(\mathbf{r}_{G,1} + \mathbf{s}) + c_I^{(3)}(\mathbf{r}_{G,1} + \mathbf{s}) + \dots. \tag{4.12}$$

The lowest-order term in (4.12) can be explicitly written as

$$\begin{aligned} c_I^{(0)}(\mathbf{r}_{G,1} + \mathbf{s}) &= \frac{1}{D} \int_q G_q [A_1 S_q^{(1)} e^{i\mathbf{q}\cdot\mathbf{r}_{G,1}} + A_2 S_q^{(2)} e^{i\mathbf{q}\cdot\mathbf{r}_{G,2}}] e^{-i\mathbf{q}\cdot(\mathbf{r}_{G,1} + \mathbf{s})} \\ &= \frac{A_1}{D} [Q_1^{(0)}(s) + Q_1^{int}(\theta, \varphi)], \end{aligned} \tag{4.13}$$

where the terms correspond to the respective terms in (4.8); the first term arises from self-production of the chemical concentration while the second term is from the interaction. The first term $Q_n^{(0)}(s)$ is

$$\begin{aligned} Q_n^{(0)}(s) &= \int_q G_q^n S_q e^{-i\mathbf{q}\cdot\mathbf{s}} \\ &= \frac{2R_0^2}{\pi} \int_0^\infty dq G_q^n q j_1(qR_0) j_0(qs). \end{aligned} \tag{4.14}$$

There is no angular dependence, and thus this term describes an isotropic concentration field. Without hydrodynamic flow and the resulting motion of the drops, our model is isotropic, and therefore, the lowest-order concentration field must be isotropic. Nevertheless, as we will see, the coupling to the flow field or perturbation of the concentration field by another drop would result in an anisotropic concentration field, which would then lead to an inhomogeneous surface tension and self-propulsion. The contribution from interaction, $Q_n^{int}(\theta, \varphi)$ in (4.13) can be calculated as

$$\begin{aligned} Q_n^{int}(s) &= \frac{A_2}{A_1} \int_q G_q S_q e^{-i\mathbf{q}\cdot(\mathbf{s} + \mathbf{r}_{G,1} - \mathbf{r}_{G,2})} \\ &= \frac{2R_0^2 A_2}{\pi A_1} \int_0^\infty dq G_q^n q j_0(q|\mathbf{s} + \mathbf{r}_{G,1} - \mathbf{r}_{G,2}|) j_1(qR_0). \end{aligned} \tag{4.15}$$

Using the addition theorem of spherical Bessel functions (Watson 1922), we have

$$j_0(q|\mathbf{s} + \mathbf{r}_{G,1} - \mathbf{r}_{G,2}|) = \sum_{l=0}^\infty (2l + 1) j_l(qs) j_l(qr_{12}) P_l(\cos \phi_{s12}), \tag{4.16}$$

where $r_{12} = |\mathbf{r}_{G,2} - \mathbf{r}_{G,1}|$ and ϕ_{s12} is the angle between \mathbf{s} and $\mathbf{r}_{12} = \mathbf{r}_{G,2} - \mathbf{r}_{G,1}$. The Legendre polynomial can be decomposed as follows (Arfken, Weber & Weber 1968):

$$P_l(\cos \phi_{s12}) = \frac{4\pi}{2l+1} \sum_{m=-l}^l Y_l^m(\theta, \varphi) Y_l^{m*}(\theta_{12}, \varphi_{12}). \quad (4.17)$$

Then (4.15) becomes

$$Q_n^{int}(\mathbf{s}) = \frac{8R_0^2 A_2}{A_1} \sum_{l=0}^{\infty} \sum_{m=-l}^l \int_0^{\infty} dq G_q^n q j_1(qR_0) j_l(qs) j_l(qr_{12}) Y_l^m(\theta, \varphi) Y_l^{m*}(\theta_{12}, \varphi_{12}). \quad (4.18)$$

This concentration field, (4.13) and (4.18), becomes anisotropic, since it contains $Y_l^m(\theta, \varphi)$. This arises from the coupling of the relative position $Y_l^{m*}(\theta_{12}, \varphi_{12})$ to the concentration field created by another drop in contrast with the isotropic term of (4.15).

In expansion of the concentration field, (4.12), the next-order term is

$$\begin{aligned} c_l^{(1)}(\mathbf{r}_G + \mathbf{s}) &= -\frac{A_1}{D^2} \int_q G_q^2 \left[(\mathbf{i}q \cdot \mathbf{u}^{(1)}) S_q^{(1)} e^{iq \cdot \mathbf{r}_{G,1}} + \frac{A_2}{A_1} (\mathbf{i}q \cdot \mathbf{u}^{(2)}) S_q^{(2)} e^{iq \cdot \mathbf{r}_{G,2}} \right] e^{-iq \cdot (\mathbf{r}_G + \mathbf{s})} \\ &= u_i^{(1)} \frac{A_1}{D^2} \left[n_i^{(0)} \frac{\partial Q_2^{(0)}}{\partial s} \right] + u_i^{(2)} \frac{A_2}{D^2} \frac{\partial}{\partial s_i} Q_2^{int}, \end{aligned} \quad (4.19)$$

where the first term arises from the source term of the first drop and thus is the same as the velocity without the second drop. In contrast with the lowest-order concentration $c_l^{(0)}$, both of the terms in (4.19) are anisotropic. In the first term, this is because the coupling to the velocity of the drop ($\mathbf{u}^{(1)}$) and the concentration field. Since the drop is moving, the produced concentration field remains at the back of the drop, leading different concentrations between at the front and rear (Yabunaka *et al.* 2012). In the second term, both the velocity of the drop and the interaction produce an anisotropic concentration.

The velocity in (4.3) is expressed by the sum of the velocity due to the normal and tangential forces in (3.9) on the surface of the drop. Each force is the sum of the force for an isolated drop and the contribution from the interaction:

$$\mathbf{u}_0 + \mathbf{u}_c = \mathbf{u}_1 + \mathbf{u}_2, \quad (4.20)$$

where \mathbf{u}_1 and \mathbf{u}_2 are the contributions from the normal and tangential forces, respectively. The velocities can be decomposed as follows:

$$\mathbf{u}_1 = \mathbf{u}_1^{(0)} + \mathbf{u}_1^{int} \quad (4.21)$$

$$\mathbf{u}_2 = \mathbf{u}_2^{(0)} + \mathbf{u}_2^{int}. \quad (4.22)$$

The Stokes equation (3.9) is solved by using the Oseen tensor,

$$T_{ij} = \frac{1}{8\pi\eta} \left[\frac{1}{r} \delta_{ij} + \frac{x_i x_j}{r^3} \right] \quad (4.23)$$

and the interaction can be expanded with respect to the magnitude of the velocity of the second drop corresponding to each order in the expansion of (4.12): $\mathbf{u}_1^{int} =$

$\mathbf{u}_1^{int,0} + \mathbf{u}_1^{int,1} + \mathbf{u}_1^{int,2} + \dots$. The lowest-order contribution from the interaction between spherical drops to the velocity is obtained from (4.13) and (4.18):

$$\begin{aligned} u_{i,1}^{int,0} &= \frac{\gamma_c R_0}{\Omega} \int da \int da' n_i(a) T_{jk}(a, a') n_j(a) n_k(a') \left(-\frac{2}{R_0}\right) c_i^{(0)}(a') \\ &= -\frac{64\gamma_c R_0^2 A_2 a_{1,0}^{(1)}}{15\eta D} \int_0^\infty dq q G_q j_1(qR_0) j_1(qr_{12}) j_1(qR_0) N_i(\theta_{12}, \varphi_{12}), \end{aligned} \tag{4.24}$$

where $a_{1,0}^{(1)} = 3/(4\pi)$ and

$$N(\theta_{12}, \varphi_{12}) = \hat{\mathbf{r}}_{12} = \frac{\mathbf{r}_{12}}{|\mathbf{r}_{12}|} = \frac{\mathbf{r}_{2,G} - \mathbf{r}_{1,G}}{|\mathbf{r}_{2,G} - \mathbf{r}_{1,G}|} \tag{4.25}$$

is the normal vector pointing the second drop from the first drop. The velocity due to the tangential force is

$$\begin{aligned} u_{i,2}^{int,0} &= \frac{\gamma_c R_0}{\Omega} \int da \int da' n_i(a) T_{jk}(a, a') n_j(a) [\delta_{ki} - n_k(a') n_i(a')] \nabla_l c_l^{(0)} \\ &= \frac{\gamma_c R_0^2}{5\Omega\eta} \int da' [\delta_{ij} - n_i(a') n_j(a')] \nabla_j c_i^{(0)}(a'). \end{aligned} \tag{4.26}$$

In (4.13), the first contribution, which comes from $Q_1^{(0)}(s)$, vanishes since $(\delta_{ij} - n_i(a') n_j(a')) n_j = 0$. This is obvious since the concentration field in (4.14) is isotropic. The second contribution comes from $Q_1^{int}(\theta, \varphi)$ in (4.13) and is given by

$$u_{i,2}^{int,0} = \frac{8\gamma_c R_0^3 A_2 a_{0,1}^{(1)}}{5\eta D} \int_0^\infty dq q G_q j_1(qR_0) j_1(qr_{12}) j_1(qR_0) N_i(\theta_{12}, \varphi_{12}), \tag{4.27}$$

where $a_{0,1}^{(1)} = (2/R_0) a_{1,0}^{(1)}$. Both (4.24) and (4.27) are along the direction of the centreline between the two drops. This originates from the anisotropic concentration field created by the isotropic field around the other drop. Combining (4.24) and (4.27), we obtain

$$\begin{aligned} \mathbf{u}_c &= -\nabla_{\mathbf{r}_1} U_0(r_{12}) \\ &= -\frac{\gamma_c A_2}{\eta D \beta^2} k_1(\beta r_{12}) g_0(\beta R_0) \frac{\mathbf{r}_2 - \mathbf{r}_1}{|\mathbf{r}_2 - \mathbf{r}_1|}, \end{aligned} \tag{4.28}$$

where $k_n(x)$ is the modified spherical Bessel function of the second kind, defined as $k_n = (-1)^n x^n (d/(x dx))^n (\exp(-x)/x)$. The interaction may be expressed as if there is the following potential:

$$U_0(r_{12}) = \frac{16a_{1,0}^{(1)} \gamma_c R_0^2 A_2}{15\eta D} \int_0^\infty dq G_q j_1(qR_0) j_0(qr_{12}) j_1(qR_0). \tag{4.29}$$

Here we have used (A 4). Using (A 5) and (A 7), we obtain

$$U_0(r_{12}) = \frac{\gamma_c A_2}{\eta D \beta^3} g_0(\hat{R}_0) k_0(\beta r_{12}), \tag{4.30}$$

with $\hat{R}_0 = \beta R_0$. For given parameters, the potential decays exponentially at large distance between the two drops as $U_0 = \tilde{U}_0 k_0(\beta r_{12})$ as shown figure 3(a). The

magnitude of the potential $\tilde{U}_0 = \gamma_c A_2 / (\eta D \beta^3) g_0(\hat{R}_0)$ depends on the parameters and the size of the drop. The size dependence is explicitly given by

$$g_0(\hat{R}_0) = -\frac{2a_{1,0}^{(1)}\pi}{15\hat{R}_0^2} [-2(\hat{R}_0^2 + 2) \cosh(2\hat{R}_0) + 5\hat{R}_0 \sinh(2\hat{R}_0) + 4]. \quad (4.31)$$

The plot of g_0 is shown in figure 3. From (3.14), the activity of the first drop is controlled by $\gamma_c A_1$. In order to exhibit the instability for an isolated drop, the activity $\gamma_c A_1$ must be positive. In that case, the inequality $g_0(\hat{R}_0) \geq 0$ implies that the potential is repulsive when $A_1 A_2 > 0$ and attractive when $A_1 A_2 < 0$.

4.3. Far-field approximation

When the distance between two drops is significantly larger than the size of the drops and the scaled radius is very small, we may simplify the calculation of the previous section. For $r_{12} \gg R_0$, we have the following approximation

$$|\mathbf{s} - \mathbf{r}_{12}| = r_{12} \left[1 + \frac{s^2}{r_{12}^2} - \frac{2\mathbf{s} \cdot \mathbf{r}_{12}}{r_{12}^2} \right]^{1/2} \simeq r_{12} \left[1 - \frac{\mathbf{s} \cdot \mathbf{r}_{12}}{r_{12}^2} + \left(\frac{s^2}{2r_{12}^2} - \frac{(\mathbf{s} \cdot \mathbf{r}_{12})^2}{2r_{12}^4} \right) + \dots \right]. \quad (4.32)$$

Instead of using (4.16), for $\beta R_0 \ll 1$, we may use the following expansion:

$$j_0(q|\mathbf{s} - \mathbf{r}_{12}|) \simeq j_0(qr_{12}) - qr_{12} j_0'(qr_{12}) \frac{\mathbf{s} \cdot \mathbf{r}_{12}}{r_{12}^2} + \frac{qr_{12}}{2} \left[j_0'(qr_{12}) \frac{s^2}{r_{12}^2} + (-j_0'(qr_{12}) + qr_{12} j_0''(qr_{12})) \frac{(\mathbf{s} \cdot \mathbf{r}_{12})^2}{r_{12}^4} \right] + \dots \quad (4.33)$$

With this expansion, we will use (4.15) instead of (4.18). If we take only the zeroth-order term in the expansion of the concentration field, the velocity of the drop due to the normal force becomes

$$\mathbf{u}_{i,1}^{int,0} = -\frac{16R_0^3 \gamma_c A_2}{15\pi \Omega \eta D} \int da' n_i^{(0)}(a') \int dq G_q q j_0(q|\mathbf{R}(a') - \mathbf{r}_{12}|) j_1(qR_0). \quad (4.34)$$

For the spherical drop, $\mathbf{R}(a') = R_0 \mathbf{n}(a')$, and therefore, in (4.33), the terms which contain an even number of s do not contribute to the integral. The isotropic term in (4.33) does not make a contribution for $c_i^{(0)}$. For the lowest-order approximation, the velocity becomes

$$\mathbf{u}_{i,1}^{int,0} \simeq -\frac{16R_0^2 \gamma_c A_2}{15\pi \eta D} N_i(\theta_{12}, \varphi_{12}) \int dq G_q q^2 R_0 j_1(qr_{12}) j_1(qR_0). \quad (4.35)$$

The contribution from the tangential force is

$$\begin{aligned} \mathbf{u}_{i,2}^{int,0} &= \frac{\gamma_c R_0^2 A_1}{5\Omega \eta D} \int da' [\delta_{ij} - n_i^{(0)}(a') n_j^{(0)}(a')] \nabla_j Q_1^{int} \\ &= \frac{4\gamma_c R_0^3 A_2}{5\pi \eta D} N_j(\theta_{12}, \varphi_{12}) \int dq G_q q^2 j_1(qR_0) j_1(qr_{12}). \end{aligned} \quad (4.36)$$

Under the far-field approximation, we obtain the interaction $\mathbf{u}_c \sim k_1(\beta r_{12}) \mathbf{N}$, which is similar to that of (4.28), and the potential $U_0 \sim k_0(\beta r_{12})$, which is similar to that

of (4.30), although we have a different functional form for $g_0(\beta R_0)$. Figure 3(a) shows $g_0(\beta R_0)$ in (4.28) and that obtained under the far-field approximation. When $\beta R_0 \ll 1$, the two results agree, although they deviate when $\beta R_0 \gg 1$, since in that case, the far-field expansion is not justified.

We can analytically confirm that (4.28) approaches the above expression of $u_i^{int,0}$ in the far-field limit $r_{12} \gg R_0$ and $\beta R_0 \ll 1$, by using the following relation, which holds in the far-field limit:

$$3 \int dq q G_q (j_1(qR_0))^2 j_1(qr_{12}) \simeq R_0 \int dq q^2 G_q j_1(qR_0) j_1(qr_{12}). \tag{4.37}$$

We can systematically compute the terms that are higher order with respect to the magnitude of the velocity of the second drop. For the first-order term in the expansion, the velocity is expressed as

$$u_{i,1}^{int,1} = -\frac{8R_0 \gamma_c A_2}{15 \Omega \eta D^2} u_j^{(2)} \int da' n_i^{(0)}(a') \frac{\partial}{\partial s_j} Q_2^{int}. \tag{4.38}$$

Similarly, the other higher-order terms in the expansion contain higher derivatives with respect to s_i . At the far-field limit, the first term in (4.33) does not depend on s_i and therefore, in the higher-order terms, the gradient with respect to s_i vanishes. At the next order, Q_n^{int} is linear in s and therefore the higher-order terms do not contribute to the velocity. The higher-order terms start to appear beginning with the third term in (4.33). The same argument can also be applied to the tangential force. From the symmetry, this term should vanish for the second term in (4.33). Indeed, the integral has an odd number of normal vectors and thus it vanishes. We note that although we have considered only a spherical drop, in the general case, the shape of the first drop may affect its velocity. Consequently, the interaction cannot be expressed in the simple form as a potential, as in (4.28).

5. Collision of two particles

In the previous sections, we have discussed two-body interactions. The results give kinetic rules for the position ($\mathbf{x}^{(\alpha)}$) and velocity ($\mathbf{u}^{(\alpha)}$) of the α th drop ($\alpha = 1, 2$). We assume there is no viscosity contrast, that is, $\eta^{(o)} = \eta^{(i)}$. The kinetic equations are

$$\frac{d\mathbf{x}^{(1)}}{dt} = \mathbf{u}^{(1)} \tag{5.1}$$

$$m \frac{d\mathbf{u}^{(1)}}{dt} = (\tau - \tau_c) \mathbf{u}^{(1)} - g |\mathbf{u}^{(1)}|^2 \mathbf{u}^{(1)} + \tau_c (\mathbf{u}_c + \mathbf{u}_h), \tag{5.2}$$

where the interactions due to concentration overlap and hydrodynamics are, respectively,

$$\mathbf{u}_c = -\nabla_{r_1} U_0(r_{12}) = -\frac{\gamma_c A_2}{\eta D \beta^2} g_0(\beta R_0) k_1(\beta r_{12}) \mathbf{N} \tag{5.3}$$

$$\mathbf{u}_h = \left(\frac{R}{r_{12}}\right)^3 \left[-\frac{1}{2} \delta_{ij} + \frac{3}{2} \mathbf{N} \mathbf{N}\right] \cdot \mathbf{u}^{(2)} + O\left(\left(\frac{R}{r_{12}}\right)^2 \mathbf{S}^{(2)} \cdot \mathbf{N}\right), \tag{5.4}$$

where the directional vector is from the first drop and points toward the second drop (4.25). The coefficients m , τ and g are found in Yabunaka *et al.* (2012). Note

that (5.2) is an equation for velocity since the effective mass m has the dimension of time. The equation of motion for the second drop is obtained by interchanging the indices $1 \leftrightarrow 2$. S_{ij} is the dipolar concentration distribution created around the drop, $S_{ij} = (R_0/\Omega) \int [n_i(a)n_j(a) - (1/3)\delta_{ij}]c(a) da$. This second moment of the concentration field arises both from ellipsoidal deformation and self-propulsion (Yoshinaga 2014). Since we consider a spherical drop and assume the system is close to the drift bifurcation point, $S_{ij} \sim \epsilon^2$, the contribution of the second term in (5.4) is negligible.

The sign of the coefficients is $-(\gamma_c A_2)/(\eta D \beta^2) g_0(\beta R_0) k_1(\beta r_{12}) < 0$ when $\gamma_c A_2 > 0$. From (3.14) and (4.31), the self-propelled first drop (above the drift bifurcation) feels the interaction potential created by the second drop. The two drops repel each other when both produce or both consume chemicals. When the chemical reactions of the two drops have opposite signs, the interaction has the opposite sign and the two drops are mutually attracted. The interaction decays exponentially, as shown in figure 3(a). As the size of the drop increases, the concentration gradient associated with the concentration-mediated interaction becomes stronger at the fixed position. When the two drops approach, the interaction is best evaluated at β^{-1} , which is outside the interface of the drops. For a larger drop, the concentration field is strongly screened, and the interaction becomes weaker. Therefore, the concentration-mediated interaction u_c is most effective at $\beta R_0 \simeq 1$. In figure 3(b), the hydrodynamic interaction u_h evaluated at the distance of the characteristic length $r_{12} = 2R_0 + \beta^{-1}$ is shown for different values of the steady velocity. This distance corresponds to the situation in which the gap between the two drops is β^{-1} . As the system gets closer to the critical point, the steady velocity decreases, and the hydrodynamic interaction becomes weaker. On the other hand, the leading order of the interaction mediated by the concentration is independent from the steady velocity. Therefore, near the critical point, the interaction is dominated by the concentration field and not by the hydrodynamic interaction.

For a head-on collision, the relative position $\xi = z^{(1)} - z^{(2)}$ between the two drops is obtained from (5.1) and (5.2):

$$m\ddot{\xi} = \dot{\xi} \left(\tau - \tau_c - \frac{g}{4} \dot{\xi}^2 \right) - \tau_c \left(2U'_0(\xi) + \left(\frac{R}{\xi} \right)^3 \dot{\xi} \right), \quad (5.5)$$

where $\dot{\xi} = d\xi/dt$. The hydrodynamic interaction is repulsive before the collision. However, after the collision, and when the two drops move away from each other, the interaction becomes attractive. This contrasts with the behaviour seen in an isotropic concentration-mediated interaction. Near the critical point, the steady velocity of a drop is small, and thus the interaction created by the concentration field is stronger than that created by the hydrodynamics. Trajectories and velocity of the solution of (5.5) are shown in § 7 together with the numerical results. Although the assumptions that we have made in the calculation of the interactions are not completely justified especially during collision, we will show in the following sections that this is in semi-quantitative agreement with our numerical results.

When the motion of two drops is confined in the xz -plane, and the collision has a symmetry with respect to the x -axis, the dynamics is expressed by $\xi = z^{(1)} - z^{(2)}$ and $\rho = x^{(1)} + x^{(2)}$, as follows:

$$m\ddot{\xi} = \dot{\xi} \left(\tau - \tau_c - \frac{g}{4} (\dot{\xi}^2 + \dot{\rho}^2) \right) - \tau_c \left(2U'_0(\xi) + \left(\frac{R}{\xi} \right)^3 \dot{\xi} \right) \quad (5.6)$$

$$m\ddot{\rho} = \dot{\rho} \left(\tau - \tau_c - \frac{g}{4}(\xi^2 + \dot{\rho}^2) \right) - \frac{\tau_c}{2} \left(\frac{R}{\xi} \right)^3 \dot{\rho}. \quad (5.7)$$

Two drops collide with an incident angle θ_0 and a final angle θ_f (figure 4a). Trajectories of the solution of (5.6) and (5.7) for $\theta_0 = \pi/4$ are shown in figure 4(c). The parameters are chosen to be the same as the numerical simulations for $\eta = 2.3$. During the collision, the direction of motion changes from the incident angle, θ_0 , and it reaches the final angle, θ_f (figure 4d). The final angle is dependent on the incident angle, as shown in figure 4(b). When the incident angle is between 0 and π , the final angle is smaller than the incident angle. The hydrodynamic interaction enhances this effect; the final angle is less smaller than the incident angle if we eliminate the hydrodynamic interaction. On the other hand, if we eliminate the concentration-mediated interaction, two drops always align.

6. Numerical simulations: single drop

We numerically solve (3.2), which gives the dynamics of a drop and (3.9), which gives the flow field. We used the following equation for the dynamics of the concentration field similar to (4.1):

$$\frac{\partial c}{\partial t} + \mathbf{v} \cdot \nabla c = D\nabla^2 c - \kappa c + \frac{1}{2}A(\phi(\mathbf{r}) + 1). \quad (6.1)$$

We assumed an axisymmetric system in which the motion of the drop was confined along the z -axis. The entire space was discretized in cylindrical coordinates, with $N_z = 96$ and $N_r = 48$ mesh points in the z - and radial (r -) directions, respectively. The mesh size was chosen to be $\Delta z = \Delta r = 1$, and the time step was $\Delta t = 0.002$. Equations (6.1) and (3.2) were discretized by using the forward Euler method. We imposed a periodic boundary condition in the z -direction, and, at $r = N_r$, we imposed the slip boundary condition $\partial_r v_z = 0$ and $v_r = 0$, the non-wetting boundary condition $\partial_r \phi = 0$, the no-flux boundary condition $\partial_r (\delta f / \delta \phi) = 0$, and $\partial_r c = 0$. The Stokes equation was solved by using the relaxation method; for a given force $\mathbf{f}(\mathbf{r})$, (3.9) was solved by introducing the virtual time derivative $d\mathbf{v}/dt$ and relaxing until a steady state was obtained. At each step in the virtual time domain, the pressure was relaxed to the steady value so that the incompressibility condition was satisfied. For the discretization, we employed the staggered lattice method, in which the r and z components of the flux were defined at the lattice points $((i + 1/2)\Delta r, j\Delta z)$ and $(i\Delta r, (j + 1/2)\Delta z)$, respectively, for $i = 0, \dots, N_r - 1$ and $j = 0, \dots, N_z - 1$. In order to quickly prepare initial conditions that are stationary under (6.1) and (3.2) with $\mathbf{v} = 0$, we solved the following equations

$$\frac{\partial c}{\partial t'} = \alpha \left[D\nabla^2 c - \kappa c + \frac{1}{2}A(\phi(\mathbf{r}) + 1) \right], \quad (6.2)$$

$$\frac{\partial \phi}{\partial t'} = -\frac{\delta F}{\delta \phi} + \left\langle \frac{\delta F}{\delta \phi} \right\rangle, \quad (6.3)$$

with $\alpha = 20$ and $\Delta t' = 0.01$ until $t' = 160$, starting from $c = 0$ and $\phi = -\tanh(R - |\mathbf{r} - \mathbf{r}_{G,1}|) + 0.05$ at $t' = 0$. We added a small-amplitude noise to this initial condition in order to investigate the self-propelled motion of a drop with spontaneous symmetry breaking.

First, we dropped the advection term in (6.1) in order to directly compare our numerical results with the theoretical predictions of Yabunaka *et al.* (2012). We

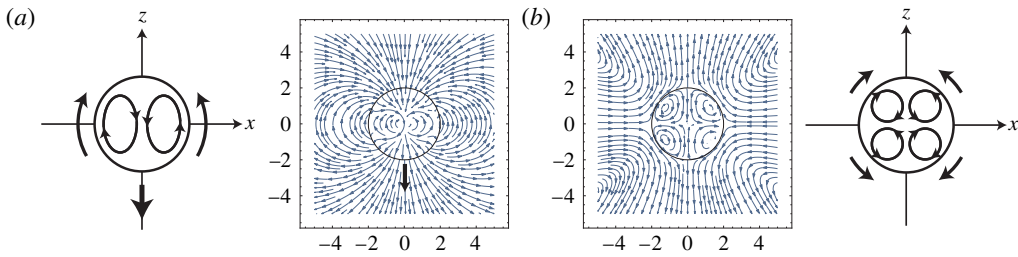


FIGURE 1. (Colour online) The flow field created by an isolated drop. (a) The $l=1$ mode associated with the translational motion under $\gamma_{1,0} > 0$, as given by (2.15) and (2.16). The direction of motion is indicated by the thick arrow. (b) The $l=2$ mode of the dipolar flow for $\gamma_{2,0} > 0$, as given by (2.19) and (2.20). The schematic drawings of the flow fields are also shown.

varied the viscosity η to realize self-propulsive motion under fixed $R = 16$, $B_0 = 0.2$, $B_1 = 0.5$, $D = 0.5$, $A = 0.08$, $\kappa = 0.005$ and $L = 1$. Here $\beta = \sqrt{\kappa/D} = 0.1$. We confirmed that this choice of parameters satisfies the assumptions listed following (3.10). With these parameters, the critical value of the viscosity is theoretically predicted as $\eta_c \simeq 1.742$ when using (3.14). We will discuss possible reasons for the discrepancies between the numerical results and the theoretical predictions in detail in §7. In order to estimate the critical value, we need to evaluate the surface tension and γ_c . When the interface is sharp and the value of $c(\mathbf{r})$ at the interface is unique, then $\gamma = (2\sqrt{2B(c)}/3)$ and $\gamma_c = (\sqrt{2B_1}/3\sqrt{B(c)})$. However, since we use a diffuse-interface model, the concentration at the interface region varies in space. The surface tension is

$$\gamma = \int B(c) \left(\frac{\partial \phi}{\partial n} \right)^2 dn, \quad (6.4)$$

where $\partial/\partial n$ is the spatial derivative along the direction normal to the interface. We numerically estimated (6.4) and compared the results with (3.8) to obtain $\gamma_c \sim 0.510$.

When $\eta < \eta_c$, the stationary state becomes unstable, and the drop starts to move. The velocity of the drop gradually increases until it reaches a steady state, as shown in figure 5. During the self-propulsive motion, the concentration field is distorted around the drop, as shown in figure 6. Clearly, the two centres of mass (that of the drop and that of the concentration) are shifted, and thus the symmetry is broken for the $\pm z$ directions. The velocity field during the motion is shown in figure 6. The velocity field in the drop frame shows a circular flow that corresponds to the $l=1$ mode in figure 1. Around the drop, the velocity field decays faster than $1/r$, suggesting that the motion is generated by the source dipole and not by a Stokeslet.

When the viscosity η is close to the critical value, the relaxation of the velocity is monotonic and well fitted with (3.17). This is consistent with the theoretical result of (3.15). When η is much smaller than the critical value, however, the relaxation of the velocity is not monotonic but has a small oscillation, as seen for $\eta = 1.7$ in figure 5. This may arise from the involvement of an additional time scale, and the truncation of the expansion of (4.10) is not completely satisfied. The steady velocity and the relaxation time are plotted in figure 7. As the viscosity η decreases, that is, as τ_c decreases, the self-propulsive speed increases. As suggested in figure 7(b,d), close to the critical point, the speed increases as $u \sim |\eta_c - \eta|^{1/2}$, which is predicted by the theory in (3.15). Figure 8 shows the relaxation time of the numerical simulations. As

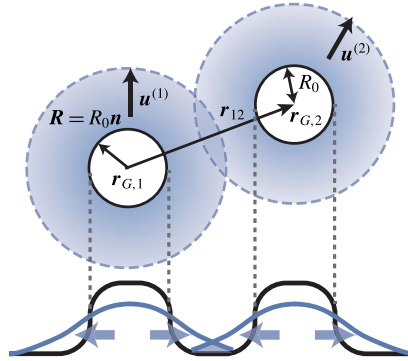


FIGURE 2. (Colour online) A schematic representation of interacting spherical drops. Each drop produces an outer concentration field. The black line shows the drop described by the field $\phi(\mathbf{r})$. The blue (grey) lines indicate the concentration fields that are independently created by each drop. The total concentration field $c(\mathbf{r})$ contains the overlap between the two fields and the two drops interact through this field. At the bottom is a side view of the fields $\phi(\mathbf{r})$ and $c(\mathbf{r})$.

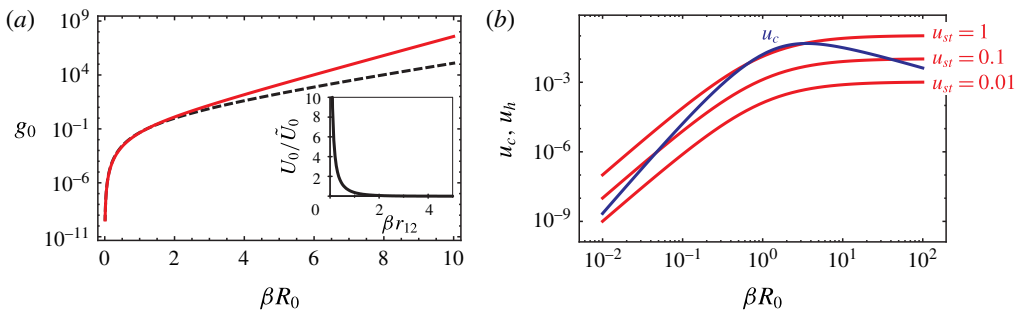


FIGURE 3. (Colour online) (a) Semilogarithmic plot of the normalized concentration-mediated interaction as a function of the normalized size of the drop, βR_0 . The solid (red) line shows $g_0(\beta R_0)$, as in (4.28), and the dashed (black) line corresponds to the result under the far-field approximation. Inset: the interaction potential $U_0/\tilde{U}_0 = k_0(\beta r_{12})$ as a function of the distance between the two drops when $A_1 A_2 > 0$. (b) Log-log plot of the typical hydrodynamic u_h and concentration-mediated u_c interactions for drops of different normalized sizes (βR_0). The interactions are evaluated at the characteristic length scale $r_{12} = 2R_0 + \beta^{-1}$. For the hydrodynamic interaction, the steady velocity of the second drop without interactions is decreased from the top to the bottom line.

the viscosity approaches the critical value from below, the relaxation time diverges. This behaviour is also consistent with our theory in (3.17).

We evaluate the scaled coefficients m , τ and g (\hat{m} , $\hat{\tau}$, \hat{g} in Yabunaka *et al.* (2012)) by comparison with the numerical results, as follows. In terms of the non-scaled coefficients M , T and G (m , τ , g in Yabunaka *et al.* (2012)), the relaxation time and the steady velocity are expressed, respectively, as

$$s_r = \frac{M}{T - 1} \tag{6.5}$$

$$u_{st} = \sqrt{\frac{T - 1}{G}}. \tag{6.6}$$

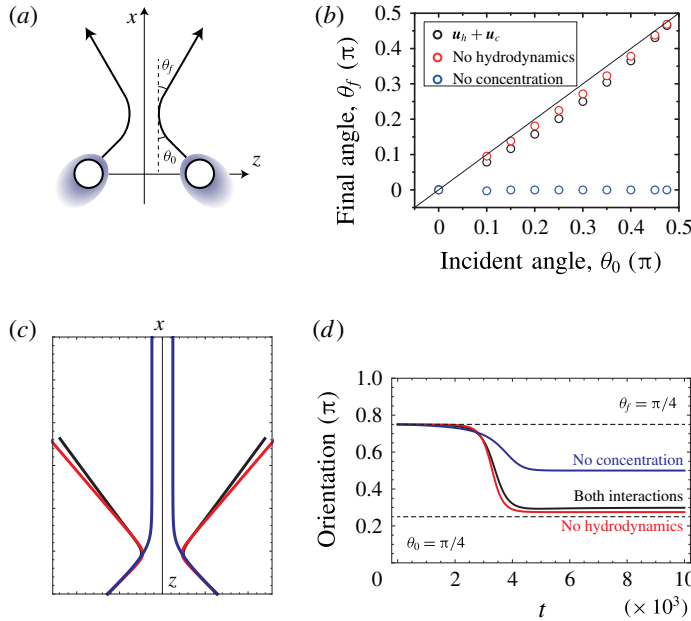


FIGURE 4. (Colour online) (a) A schematic representation of a collision, (b) the incident, θ_0 , and final, θ_f , angles for the solution of (5.6) and (5.7) (black), without the hydrodynamic interaction (red), and without the concentration-mediated interaction (blue), (c) the trajectories during the collisions for $\theta_0 = \pi/4$ and (d) the direction of motion during the collisions for $\theta_0 = \pi/4$.

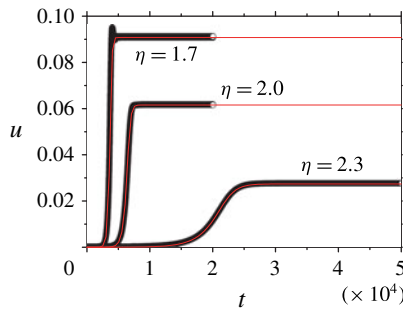


FIGURE 5. (Colour online) Self-propulsive velocity of a single drop. The velocity of the drop as a function of time is shown for numerical simulation (circles) and theory in (3.15) (line).

Since $T \sim \eta^{-1}$, the above expression for s_r predicts the divergence of the relaxation time near the threshold, which is in agreement with the numerical results in figure 8. Using $\eta_c = 2.395$, we estimate $T - 1 \sim 0.19$ for $\eta = 2.0$. From the above equations, we estimate $G \sim 49.4$ and $M \sim 96.9$. After rescaling the parameters of Yabunaka *et al.* (2012), we obtain

$$g = \tau_c(D\beta)^2 G = 0.0112, \tag{6.7}$$

$$m = MD\beta^2 \tau_c = 0.044. \tag{6.8}$$

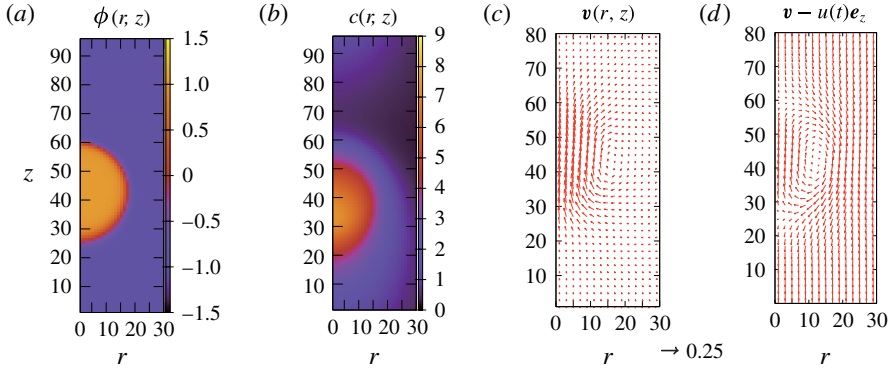


FIGURE 6. (Colour online) For a drop at steady state with $\eta = 1.5$ and $t = 3168$: (a) $\phi(\mathbf{r})$, (b) the concentration field $c(\mathbf{r})$, and (c,d) the velocity field $\mathbf{v}(\mathbf{r})$ in the laboratory frame (c) and in the drop frame (d). The self-propulsive velocity is $u = 0.109$.

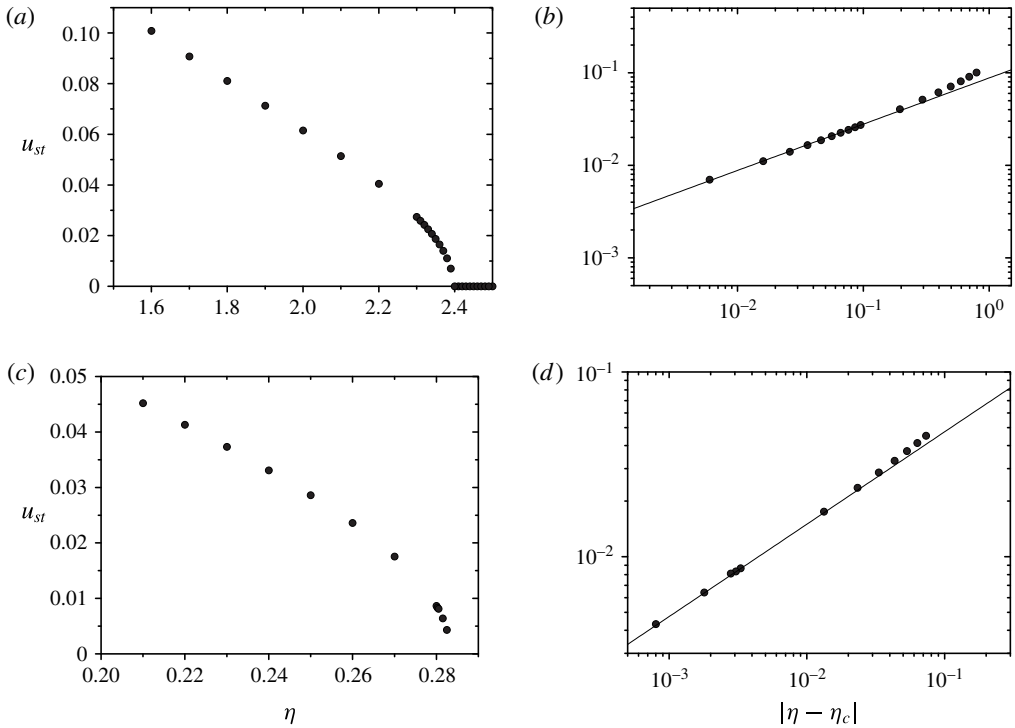


FIGURE 7. The steady velocity u_{st} with varying viscosity η (τ_c). (a,b) Without advection of the third dilute component, and (c,d) with advection. The log–log plots of the steady velocity and the distance from the critical points are shown in (b) and (d). The solid lines show the exponent $u_{st} \sim |\eta - \eta_c|^{1/2}$.

These values of m and g agree with the theoretical predictions in Yabunaka *et al.* (2012) with $\beta R = 1.6$. In the same way, we evaluated g and m for other values of η near η_c , as shown in figure 9. We found that they are almost constant, which is consistent with the theoretical predictions.

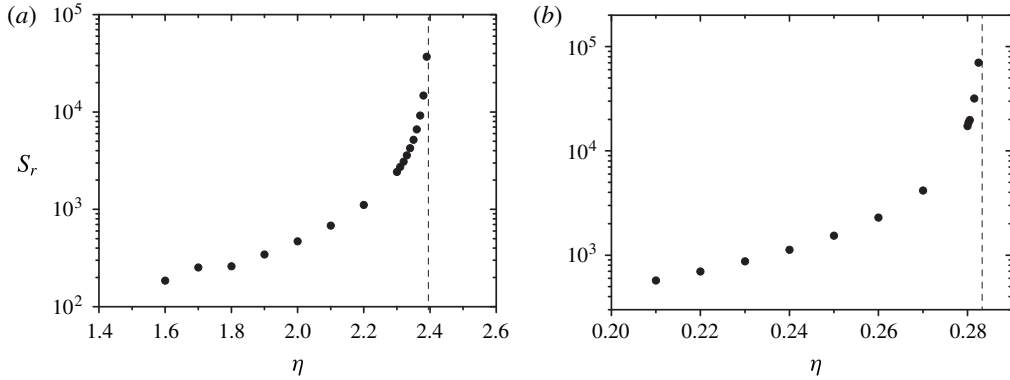


FIGURE 8. The relaxation time to reach the steady velocity. (a) Without advection of the third dilute component and (b) with advection. The vertical dashed lines correspond to the critical viscosity.

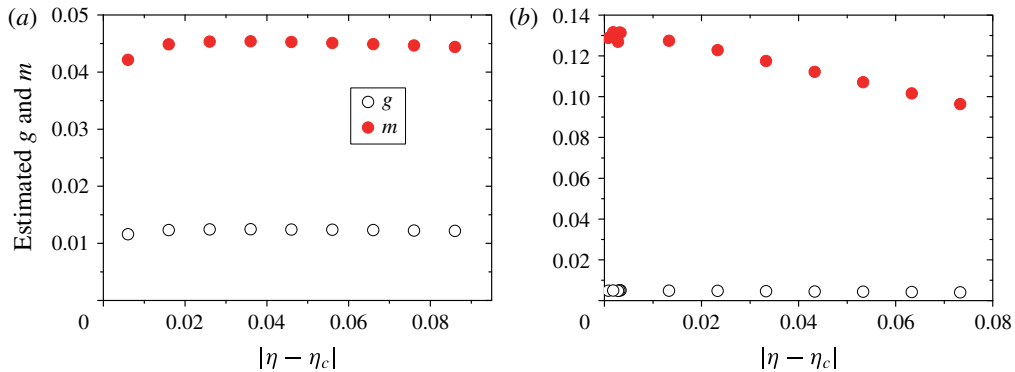


FIGURE 9. (Colour online) Numerically estimated coefficients g and m . (a) Without advection of the third dilute component, and (b) with advection.

The advection term in (6.1) does not change the qualitative features of the transition; we found that, when $\eta < \eta_c = 0.2833$, the stationary state becomes unstable, and the drop starts to move. In addition, figures 7 and 8 show that the advection does not modify the scaling behaviour of the steady velocity near the critical point. Both with and without the advection term, the steady velocity grows as $|\eta - \eta_c|^{1/2}$. The relaxation time also diverges near the bifurcation point. We note that the critical point when there is advection ($\eta_c = 0.2833$) is much smaller than when there is no advection ($\eta_c = 2.395$). In Yabunaka *et al.* (2012), the effect of the advection is only treated in the limit $\beta R \rightarrow 0$ and it is predicted that, in the presence of advection, the drift instability is suppressed, but the bifurcation behaviour will not be essentially changed. Thus, our numerical results with $\beta R = 1.6$ agree qualitatively with the theoretical prediction as $\beta R \rightarrow 0$, even though the theory does not directly apply to our case.

7. Numerical simulations: interaction

With the same numerical method that we used in the previous section for an isolated drop, we carried out numerical simulations for two drops. The entire

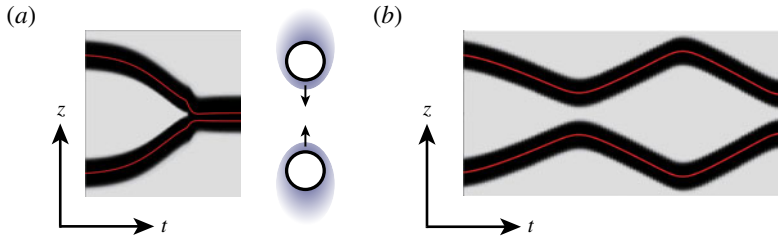


FIGURE 10. (Colour online) The trajectories of two colliding drops for (a) $\eta = 1.5$ and (b) $\eta = 2.3$. The slices of the field ϕ at $r = 0$ are superposed for the direction of time. The darker (brighter) region corresponds to $\phi = 1$ ($\phi = -1$). The solid lines show the trajectories of the centres of the drops. Because of the periodic boundary condition, the drops reaching the top or bottom boundaries are reflected by the interactions with image drops outside the simulation box.

space was discretized in cylindrical coordinates with $N_z = 200$ and $N_r = 48$ mesh points in the z - and radial (r -) directions. The mesh size was chosen to be $\Delta z = \Delta r = 1$, and the time step was $\Delta t = 0.002$ for $\eta > 1.9$ and $\Delta t = 0.001$ for $\eta < 1.9$. We prepared the initial condition in the same way, but with $\phi = \tanh(R - |\mathbf{r} - \mathbf{r}_{G,1}|) + \tanh(R - |\mathbf{r} - \mathbf{r}_{G,2}|) - 2 + 0.05$ with $\mathbf{r}_{G,1} = 29$ and $\mathbf{r}_{G,2} = 171$.

Figure 10 shows the trajectory of the two centres of mass of the interacting particles. There are two distinct dynamics for the collision: fusion, as shown in figure 10(a), and reflection, as shown in figure 10(b). When the viscosity η is far below the critical point, the two drops approach and eventually merge. On the other hand, when η is close to the critical point, the two drops do not merge even when they are approaching, but they reflect and move in opposite directions. Surprisingly, the latter collision is elastic, despite the fact that the system is dissipative. The drops move at the same speed after the collision as they did before the collision. This can be understood from our reduced description (3.10), in which friction vanishes as τ_c approaches τ ; note that τ_c is proportional to η as shown in (3.14). Thus, the drop behaves as if it were in a conserved system because of the balance between dissipation and the energy injection associated with chemical production. This is in contrast with both the squirmer and the Janus particle, since in those models, there is no inertia term in the equation of motion. We note that similar elastic behaviour has been reported for pulse collisions in reaction–diffusion systems (Ohta *et al.* 1997; Ei *et al.* 2006).

In order to clarify the origin of the interaction, we solve the reduced equation (5.5), and compare with the full numerical simulations using the same initial conditions. The additional terms, which describe the interaction with image drops, are added to (5.5) in order to take into account the periodic boundary condition used in the simulation. The parameters in (5.5) are obtained from the result of a single drop, and thus there is no fitting parameter in the equation. The result for $\eta = 2.3$ (figure 10b) is shown in figure 11(a,b). There is good agreement between the results of the reduced equation and those of the original model. We found that the overall behaviour of the evolution of \mathbf{u} is dominated by the concentration-mediated interaction, although the hydrodynamic interaction gives some correction on it. The contributions from the hydrodynamic ($\sim \xi^{-3}$) and concentration-mediated interactions ($\sim U'_0(\xi)$) are shown in figure 11. Over most of the region, u_c dominates u_h . However, the hydrodynamic interaction dominates when $\xi \gg 80$, since the hydrodynamic (concentration-mediated) interaction decays algebraically (exponentially). For $\eta = 1.5$

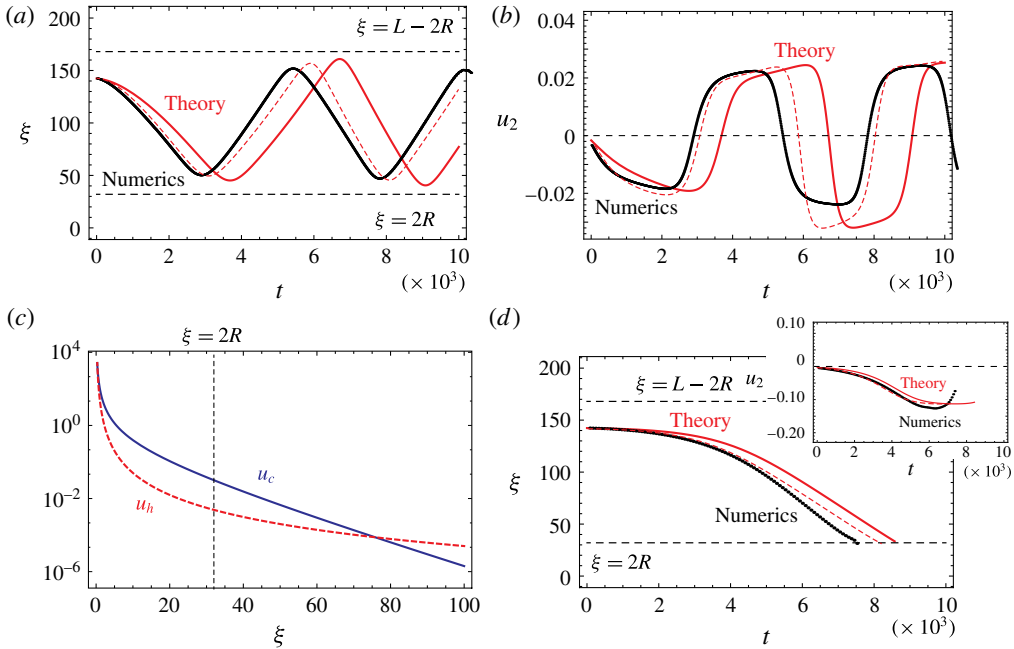


FIGURE 11. (Colour online) Comparison between the reduced equations, (5.2) and (5.5), and the full model for (a–c) $\eta = 2.3$ and (d) $\eta = 1.5$. (a) The distance $\xi = |z^{(1)} - z^{(2)}|$ between two drops as a function of time, (b) velocity of the second drop and (c) the dependence of the separation distance on the hydrodynamic u_h and concentration-mediated u_c interactions, where u_h is estimated from the steady velocity u_{st} . (d) The distance between two drops for $\eta = 1.5$ and (inset) velocity of the second drop. The dashed lines in (a,b), and (d) are obtained from our theory using $R = 18.5$ instead of $R = 16$.

(figure 10a), we solved (5.5), as shown in figure 11(d) and we found that ξ becomes smaller than $2R$, which suggests fusion of the drops and agrees with the results of the numerical simulation with the original model.

This result is consistent with the following rough estimate of the relative magnitudes of these two interactions: the magnitude of the hydrodynamic interaction is estimated to be

$$|\mathbf{u}_h| = \left(\frac{R}{\xi}\right)^3 u_j^{(2)} \sim u_{st} \left(\frac{R}{\xi}\right)^3, \quad (7.1)$$

where the typical self-propelling velocity in the steady state is given by $u_{st} \sim 0.02$. The magnitude of the concentration-mediated interaction is

$$|\mathbf{u}_c| \sim \frac{15D\beta}{2\tau_c} g_0(\hat{R}_0) k_1(\beta\xi), \quad (7.2)$$

where $g_0(\hat{R}_0 = 1.6) \sim 0.39$. If we set $\xi = 2R$ and $k_1(\beta\xi) \sim 0.0167$, then $\mathbf{u}_c \sim 0.213$ and $\mathbf{u}_h \sim 0.0025$. This also confirms that the magnitude of the concentration-overlap-mediated interaction is larger than that of the hydrodynamic interaction.

The discrepancy between theory and the numerical simulations arises for several reasons. First, our reduced description is valid only near the critical point, which

is $\eta \simeq 2.395$. We choose the parameter as close to the critical point as possible. Nevertheless, the gap ($|\eta - \eta_c| \simeq 0.1$) would lead to higher-order terms in (5.2) and accordingly in (5.5). Second, there is a small discrepancy between the steady-state velocity of a single drop and that of two drops because of the difference in the system size. We used the parameters associated with the steady velocity and relaxation time from the motion of a single drop. Third, we assumed that the distance between the two drops is large, and thus the interaction when the two drops approach is not accurately described by the reduced equations. In addition to these reasons, a drop in the diffuse-interface model has a finite width of an interface. In order to use a thin interface, we need to make fine discretization in space, and this requires a huge computational cost. The size of a drop in our model is, therefore, not accurately given. If we use a slightly larger size in our theory, the agreement between the results of the reduced equation and those of the original model becomes better (figure 11). From this observation, we speculate the main error arises from the lack of the accuracy of estimation of the size. It is also noted that both relative position and relative velocity are not instantaneous quantities, but history dependent, as in (5.5). This is because of the effective inertia term of the reduced equations. Therefore, all of these errors increase with time.

8. Discussion and summary

We have developed the theory of a collision between two self-propelled drops driven by chemical reactions. Close to the bifurcation point between stationary and self-propelled states, the collision is elastic, while away from the point, fusion occurs. The interactions originate from the hydrodynamics and the overlap of the concentration field. Both interactions are repulsive during a head-on collision if the chemical reactions of the two drops have the same sign (both producing or both consuming). We found that the concentration-mediated interaction dominates the collision dynamics. Our analytical calculation is confirmed semi-quantitatively by the numerical results.

We stress that inertia-like and nonlinear terms naturally appear in the reduced description (3.10). These effects are confirmed by the numerical results; the self-propulsion occurs above the bifurcation point at which the relaxation time diverges. The steady velocity obtained as a function of the distance from the critical point also fits with our theory. During a collision of two drops, we obtain elastic behaviour near the critical point. This is consistent with the existence of an inertia-like term. The current model has no intrinsic polarity (direction), and therefore, there is a marked difference between its collision dynamics and that of the linear squirmer model. In the latter, a change in direction is inevitably followed by a rotation, while in the current model, a change in the direction is instantaneous. It has been argued that the competition between self-propulsion and the rotational diffusion time plays a relevant role in the collective behaviour of the squirmer and Janus particles (Matas-Navarro *et al.* 2014; Cates & Tailleur 2015). Our study reveals that a symmetry-breaking swimmer may have another mechanism of competition, possibly between self-propulsion and the effect of inertia. This may lead to another phase in the collective behaviour of self-propelled particles.

Although we have focused on two-body interactions, the behaviour of many particles is an obvious next target. When many particles are confined in quasi-one-dimensional channel, they show collective drift and oscillatory motion (Ikura *et al.* 2013). Similar behaviours is reproduced by the modified model, in which fusion does not occur. We will study details of the model in future.

Our treatment of interaction is similar to the works in Golovin *et al.* (1995), Lavrenteva *et al.* (1999), although there are several differences. All these models consider the interactions between two spherical objects that are producing chemical components on their surfaces. They take into account a boundary condition on the surface and evaluate the interaction by investigating the motion due to the concentration overlap and hydrodynamics. In their first attempt (Golovin *et al.* 1995), the objects do not undergo self-propulsive motion. This corresponds to $\tau_c \rightarrow \infty$ in (5.2), and thus to $\mathbf{u} = \mathbf{u}_c + \mathbf{u}_h$ although there is an additional first-order chemical reaction in their model and our model includes a damping term of the chemicals to describe a buffering effect, which regularizes the expansion in our analysis. The main difference is that our approach uses a diffuse-interface model. When the drop domains move, this is easier to solve numerically than is the boundary-value problem. Another advantage is that our method does not rely on axisymmetry, and therefore, it can be easily extended to the non-axisymmetric case. In fact, all of the terms in the hydrodynamic interaction are anisotropic, as demonstrated in the first term of (5.4). Although the dominant interaction term for concentration overlap is isotropic, as in (5.3), the higher-order terms are anisotropic because of the coupling between the relative position and the deformation. The disadvantage of our approach is its lack of accuracy; because there is a finite width at the interface, we are not able to accurately measure the size of the drop. In addition, the near-field interaction is so far computed only by using a boundary-value approach using bispherical coordinates (Golovin *et al.* 1995) or by a lubrication analysis. Despite these limitations, we believe that our approach provides useful insights to the problem of self-propulsive drops.

We limited ourselves to the cases in which the deformation of the drop is not large. We may relax this assumption by changing the parameters and we expect that this would reveal intriguing dynamics due to the coupling between self-propulsion and deformation. We leave this as a subject for future study. This work focuses on head-on collisions in detail and suggests the importance of concentration-mediated interactions. However, there are other types of collision, such as motion that is not parallel to the centreline between two drops. In these cases, it is possible that the hydrodynamics plays a role. As described by the reduced equations (5.1)–(5.4), the dominant term in a concentration-mediated interaction is isotropic for each drop, while for a hydrodynamic interaction, it is not. When the centreline is not along the direction of the motion, that is, when the incident angle is between 0 and $\pi/2$, the anisotropic interaction results in the rotation of the drops. Our preliminary results suggest that the hydrodynamics plays a relevant role when the steady velocity is high and the deformation of the drop occurs. In the current model, fusion occurs at the high steady velocity. Nevertheless, by inhibiting fusion, we have also obtained the bound state, that is, the state in which two drops move together following a collision at a certain incident angle. This cannot be reproduced without considering the hydrodynamic interaction. The investigation of these motions is an important area for future research.

Acknowledgements

The authors are grateful to K.-I. Ueda and T. Liverpool for helpful discussions. S.Y. acknowledges support by Grants-in-Aid for Japan Society for Promotion of Science (JSPS) Fellows (grant nos 241799 and 263111) and the JSPS Core-to-Core Program ‘Non-equilibrium dynamics of soft matter and information’. The authors acknowledge support by JSPS KAKENHI grant nos JP15K17737 for S.Y., and JP26800219, JP26103503, and JP16H00793 for N.Y.

Appendix A. Spherical Bessel function

In this work, we use the spherical Bessel function defined as

$$j_n(x) = \sqrt{\frac{\pi}{2x}} J_{n+1/2}(x), \tag{A 1}$$

where $J_n(x)$ is the n th order Bessel function of the first kind. The spherical Bessel functions can also be expressed in the following way:

$$j_n(x) = (-1)^n x^n \left(\frac{1}{x} \frac{d}{dx} \right)^n \frac{\sin x}{x}. \tag{A 2}$$

The spherical Bessel function satisfies the following relation

$$j'_n(x) = \frac{n}{x} j_n(x) - j_{n+1}(x), \tag{A 3}$$

where $j'_n(x) = dj_n(x)/dx$. For $n = 0$, it becomes

$$j'_0(x) = -j_1(x). \tag{A 4}$$

We consider the following integral, which contains three spherical Bessel functions:

$$\begin{aligned} & \int_0^\infty \frac{q^m}{q^2 + \beta^2} j_l(qR_0) j_{l'}(qr_{12}) j_{l''}(qR_0) dq \\ &= (-1)^{l+l'+l''} R_0^{l+l''} r_{12}^{l'} \left(\frac{1}{R_0} \frac{\partial}{\partial R_0} \right)^l \left(\frac{1}{r_{12}} \frac{\partial}{\partial r_{12}} \right)^{l'} \left(\frac{1}{R_0} \frac{\partial}{\partial R_0} \right)^{l''} \\ & \times \int_0^\infty \frac{\sin(qR_0) \sin(qr_{12}) \sin(qR_0)}{R_0^2 r_{12} (q^2 + \beta^2) q^{l+l'+l''+3-m}} dq. \end{aligned} \tag{A 5}$$

Since $l + l' + l''$ is even and m is either $m = 0$ or $m = 2$, the integral does not change under the transformation $q \rightarrow -q$. We consider the integral

$$\begin{aligned} I &= \frac{1}{2} \int_{-\infty}^\infty \frac{\sin(qR_0) \sin(qr_{12}) \sin(qR_0)}{(q^2 + \beta^2) q^{l+l'+l''+3-m}} dq \\ &= -\frac{1}{16i} \int_{-\infty}^\infty \frac{(e^{iqR_0} - e^{-iqR_0})^2 (e^{iqr_{12}} - e^{-iqr_{12}})}{(q^2 + \beta^2) q^{l+l'+l''+3-m}} dq. \end{aligned} \tag{A 6}$$

This integral is calculated from residues $q = 0, \pm i\beta$. The main contribution arises from the residue $q = i\beta$ for the integration path passing $+\infty$ in the positive direction, and from the residue $q = -i\beta$ for the integration path passing $-\infty$ in the negative direction. For $r_{12} > 2R_0$,

$$\begin{aligned} I &= -\frac{\pi}{8} \left[\lim_{q \rightarrow i\beta} \frac{(e^{iqR_0} - e^{-iqR_0})^2 e^{iqr_{12}}}{(q + i\beta) q^{l+l'+l''+3-m}} - (-1) \lim_{q \rightarrow -i\beta} \frac{(e^{iqR_0} - e^{-iqR_0})^2 e^{-iqr_{12}}}{(q - i\beta) q^{l+l'+l''+3-m}} \right] \\ &= -\frac{\pi}{8} \left[\frac{4 \sinh^2(\beta R_0) e^{-\beta r_{12}}}{2i\beta (i\beta)^{l+l'+l''+3-m}} + \frac{4 \sinh^2(\beta R_0) e^{-\beta r_{12}}}{(-2i\beta)(-i\beta)^{l+l'+l''+3-m}} \right] \\ &= -\frac{\pi \sinh^2(\beta R_0) e^{-\beta r_{12}}}{8 i\beta (i\beta)^{l+l'+l''+3-m}}. \end{aligned} \tag{A 7}$$

Next, we consider the following general integral

$$\begin{aligned} & \int_0^\infty \frac{q^n}{(q^2 + \beta^2)^n} j_l(qR_0) j_{l'}(qr_{12}) j_{l''}(qs) dq \\ &= (-1)^{l+l'+l''} R_0^l r_{12}^{l'} s^{l''} \left(\frac{1}{R_0} \frac{\partial}{\partial R_0} \right)^l \left(\frac{1}{r_{12}} \frac{\partial}{\partial r_{12}} \right)^{l'} \left(\frac{1}{s} \frac{\partial}{\partial s} \right)^{l''} \\ & \quad \times \int_0^\infty \frac{\sin(qR_0) \sin(qr_{12}) \sin(qs)}{R_0 r_{12} s (q^2 + \beta^2)^n q^{l+l'+l''+3-m}} dq. \end{aligned} \quad (\text{A } 8)$$

We calculate the following integral

$$\begin{aligned} I_n &= \frac{1}{2} \int_{-\infty}^\infty \frac{\sin(qR_0) \sin(qr_{12}) \sin(qs)}{(q^2 + \beta^2)^n q^{l+l'+l''+3-m}} dq \\ &= -\frac{1}{16i} \int_{-\infty}^\infty \frac{(e^{iqR_0} - e^{-iqR_0})(e^{iqr_{12}} - e^{-iqr_{12}})(e^{iqs} - e^{-iqs})}{(q^2 + \beta^2)^n q^{l+l'+l''+3-m}} dq. \end{aligned} \quad (\text{A } 9)$$

For $r_{12} > s > R_0$, we obtain

$$\begin{aligned} I_n &= -\frac{\pi}{8} \left[\lim_{q \rightarrow i\beta} \frac{d^{n-1}}{dq^{n-1}} \frac{(e^{iqR_0} - e^{-iqR_0})(e^{iqs} - e^{-iqs})e^{iqr_{12}}}{(q + i\beta)q^{l+l'+l''+3-m}} \right. \\ & \quad \left. - (-1) \lim_{q \rightarrow -i\beta} \frac{d^{n-1}}{dq^{n-1}} \frac{(e^{iqR_0} - e^{-iqR_0})(e^{iqs} - e^{-iqs})e^{-iqr_{12}}}{(q - i\beta)q^{l+l'+l''+3-m}} \right]. \end{aligned} \quad (\text{A } 10)$$

REFERENCES

- ANDERSON, D. M., MCFADDEN, G. B. & WHEELER, A. A. 1998 Diffuse-interface methods in fluid mechanics. *Annu. Rev. Fluid Mech.* **30** (1), 139–165.
- ARFKEN, G. B., WEBER, H. J. & WEBER, H. J. 1968 *Mathematical Methods for Physicists*. Academic.
- BHAGAVATULA, R., JASNOW, D. & OHTA, T. 1997 Nonequilibrium interface equations: an application to thermocapillary motion in binary systems. *J. Stat. Phys.* **88** (5), 1013–1031.
- BLAKE, J. R. 1971 Self propulsion due to oscillations on the surface of a cylinder at low reynolds number. *Bull. Austral. Math. Soc.* **5** (02), 255–264.
- BODE, M., LIEHR, A. W., SCHENK, C. P. & PURWINS, H.-G. 2002 Interaction of dissipative solitons: particle-like behaviour of localized structures in a three-component reaction-diffusion system. *Physica D* **161** (1–2), 45–66.
- CATES, M. E. & TAILLEUR, J. 2015 Motility-induced phase separation. *Annu. Rev. Condens. Matter Phys.* **6** (1), 219–244.
- EI, S. I., MIMURA, M. & NAGAYAMA, M. 2006 Interacting spots in reaction diffusion systems. *J. Discrete Continuous Dyn. Syst.* **14** (1), 31–62.
- FEDOSOV, A. I. 1956 Thermocapillary motion (translated by V. Berejnov & K. Morozov). *Zh. Fiz. Khim.* **30** (2), 366–373 (see also [arXiv:1303.024](https://arxiv.org/abs/1303.024)).
- GOLOVIN, A. A., NIR, A. & PISMEN, L. M. 1995 Spontaneous motion of two droplets caused by mass transfer. *Ind. Engng Chem. Res.* **34** (10), 3278–3288.
- HETSRONI, G. & HABER, S. 1970 The flow in and around a droplet or bubble submerged in an unbound arbitrary velocity field. *Rheol. Acta* **9** (4), 488–496.
- HOHENBERG, P. C. & HALPERIN, B. I. 1977 Theory of dynamic critical phenomena. *Rev. Mod. Phys.* **49** (3), 435–479.

- HOWSE, J. R., JONES, R. A. L., RYAN, A. J., GOUGH, T., VAFABAKHSH, R. & GOLESTANIAN, R. 2007 Self-motile colloidal particles: from directed propulsion to random walk. *Phys. Rev. Lett.* **99** (4), 048102.
- IKURA, Y. S., HEISLER, E., AWAZU, A., NISHIMORI, H. & NAKATA, S. 2013 Collective motion of symmetric camphor papers in an annular water channel. *Phys. Rev. E* **88**, 012911.
- ISHIKAWA, T., SIMMONDS, M. P. & PEDLEY, T. J. 2006 Hydrodynamic interaction of two swimming model micro-organisms. *J. Fluid Mech.* **568**, 119–160.
- ISHIMOTO, K. & GAFFNEY, E. A. 2013 Squirmer dynamics near a boundary. *Phys. Rev. E* **88**, 062702.
- IZRI, Z., VAN DER LINDEN, M. N., MICHELIN, S. & DAUCHOT, O. 2014 Self-propulsion of pure water droplets by spontaneous marangoni-stress-driven motion. *Phys. Rev. Lett.* **113**, 248302.
- JEFFREY, D. J. & ONISHI, Y. 1984 Calculation of the resistance and mobility functions for two unequal rigid spheres in low-reynolds-number flow. *J. Fluid Mech.* **139**, 261–290.
- JIANG, H.-R., YOSHINAGA, N. & SANO, M. 2010 Active motion of janus particle by self-thermophoresis in defocused laser beam. *Phys. Rev. Lett.* **105**, 268302.
- KAWASAKI, K. & OHTA, T. 1983 Kinetics of fluctuations for systems undergoing phase transitions – interfacial approach. *Physica A* **118** (1–3), 175–190.
- KITAHATA, H., YOSHINAGA, N., NAGAI, K. H. & SUMINO, Y. 2011 Spontaneous motion of a droplet coupled with a chemical wave. *Phys. Rev. E* **84** (1), 015101.
- LAUGA, E. & POWERS, T. R. 2009 The hydrodynamics of swimming microorganisms. *Rep. Prog. Phys.* **72** (9), 096601.
- LAVRENTEVA, O. M., LESHANSKY, A. M. & NIR, A. 1999 Spontaneous thermocapillary interaction of drops, bubbles and particles: unsteady convective effects at low Peclet numbers. *Phys. Fluids* **11** (7), 1768–1780.
- LEVAN, M. D. 1981 Motion of a droplet with a newtonian interface. *J. Colloid Interface Sci.* **83** (1), 11–17.
- LI, G.-J. & ARDEKANI, A. M. 2014 Hydrodynamic interaction of microswimmers near a wall. *Phys. Rev. E* **90**, 013010.
- LIGHTHILL, M. J. 1952 On the squirming motion of nearly spherical deformable bodies through liquids at very small reynolds numbers. *Commun. Pure Appl. Maths* **5** (2), 109–118.
- MATAS-NAVARRO, R., GOLESTANIAN, R., LIVERPOOL, T. B. & FIELDING, S. M. 2014 Hydrodynamic suppression of phase separation in active suspensions. *Phys. Rev. E* **90**, 032304.
- MICHELIN, S., LAUGA, E. & BARTOLO, D. 2013 Spontaneous autophoretic motion of isotropic particles. *Phys. Fluids* **25** (6), 061701.
- NISHIURA, Y., TERAMOTO, T. & UEDA, K.-I. 2003 Scattering and separators in dissipative systems. *Phys. Rev. E* **67**, 056210.
- OHTA, T. 2001 Pulse dynamics in a reaction-diffusion system. *Physica D* **151** (1), 61–72.
- OHTA, T., KIYOSE, J. & MIMURA, M. 1997 Collision of propagating pulses in a reaction-diffusion system. *J. Phys. Soc. Japan* **66** (5), 1551–1558.
- PAK, O. S. & LAUGA, E. 2014 Generalized squirming motion of a sphere. *J. Eng. Math.* **88** (1), 1–28.
- PAXTON, W. F., KISTLER, K. C., OLMEDA, C. C., SEN, A., ST.ANGELO, S. K., CAO, Y., MALLOUK, T. E., LAMMERT, P. E. & CRESPI, V. H. 2004 Catalytic nanomotors: autonomous movement of striped nanorods. *J. Am. Chem. Soc.* **126** (41), 13424–13431.
- RYAZANTSEV, Y. S. 1985 Thermocapillary motion of a reacting droplet in a chemically active medium. *Fluid Dyn.* **20**, 491–495; translated from *Izv. Akad. Nauk SSSR Mekh. Zhidk. Gaza* No. 3, 180–183.
- SCRIVEN, L. E. 1960 Dynamics of a fluid interface equation of motion for Newtonian surface fluids. *Chem. Engng Sci.* **12** (2), 98–108.
- SHAO, D., RAPPEL, W.-J. & LEVINE, H. 2010 Computational model for cell morphodynamics. *Phys. Rev. Lett.* **105** (10), 108104.
- SHKLYAEV, S., BRADY, J. F. & CRDOVA-FIGUEROA, U. M. 2014 Non-spherical osmotic motor: chemical sailing. *J. Fluid Mech.* **748**, 488–520.

- SPAGNOLIE, S. E. & LAUGA, E. 2012 Hydrodynamics of self-propulsion near a boundary: predictions and accuracy of far-field approximations. *J. Fluid Mech.* **700**, 105–147.
- STONE, H. A. & SAMUEL, A. D. T. 1996 Propulsion of microorganisms by surface distortions. *Phys. Rev. Lett.* **77** (19), 4102–4104.
- THUTUPALLI, S., SEEMANN, R. & HERMINGHAUS, S. 2011 Swarming behavior of simple model squirmers. *New J. Phys.* **13** (7), 073021.
- TJHUNG, E., MARENDUZZO, D. & CATES, M. E. 2012 Spontaneous symmetry breaking in active droplets provides a generic route to motility. *Proc. Natl Acad. Sci. USA* **109** (31), 12381–12386.
- TOYOTA, T., MARU, N., HANCZYC, M. M., IKEGAMI, T. & SUGAWARA, T. 2009 Self-propelled oil droplets consuming ‘fuel’ surfactant. *J. Am. Chem. Soc.* **131** (14), 5012–5013.
- TSEMAKH, D., LAVRENTEVA, O. M. & NIR, A. 2004 On the locomotion of a drop, induced by the internal secretion of surfactant. *Intl J. Multiphase Flow* **30** (11), 1337–1367.
- USPAL, W. E., POPESCU, M. N., DIETRICH, S. & TASINKEVYCH, M. 2015 Self-propulsion of a catalytically active particle near a planar wall: from reflection to sliding and hovering. *Soft Matt.* **11**, 434–438.
- WATSON, G. N. 1922 *A Treatise on the Theory of Bessel Functions*. Cambridge University Press.
- YABUNAKA, S., OHTA, T. & YOSHINAGA, N. 2012 Self-propelled motion of a fluid droplet under chemical reaction. *J. Chem. Phys.* **136** (7), 074904.
- YAM, P. T., WILSON, C. A., JI, L., HEBERT, B., BARNHART, E. L., DYE, N. A., WISEMAN, P. W., DANUSER, G. & THERIOT, J. A. 2007 Actin myosin network reorganization breaks symmetry at the cell rear to spontaneously initiate polarized cell motility. *J. Cell Biol.* **178** (7), 1207–1221.
- YOSHINAGA, N. 2014 Spontaneous motion and deformation of a self-propelled droplet. *Phys. Rev. E* **89**, 012913.
- YOSHINAGA, N., NAGAI, K. H., SUMINO, Y. & KITAHATA, H. 2012 Drift instability in the motion of a fluid droplet with a chemically reactive surface driven by marangoni flow. *Phys. Rev. E* **86**, 016108.
- YOUNG, N. O., GOLDSTEIN, J. S. & BLOCK, M. J. 1959 The motion of bubbles in a vertical temperature gradient. *J. Fluid Mech.* **6** (03), 350–356.
- ZIEBERT, F., SWAMINATHAN, S. & ARANSON, I. S. 2012 Model for self-polarization and motility of keratocyte fragments. *J. R. Soc. Interface* **9** (70), 1084–1092.